Scientific Reports

https://doi.org/10.1038/s41598-026-38722-1

Article in Press

Electromagnetic shielding performance and mechanical properties of vermiculite-based lightweight geopolymer mortars

Received: 25 December 2025

Accepted: 30 January 2026

Published online: 09 February 2026

Cite this article as: Çelik A.İ., Tunç U., Durmuş A. *et al.* Electromagnetic shielding performance and mechanical properties of vermiculite-based lightweight geopolymer mortars. *Sci Rep* (2026). https://doi.org/10.1038/s41598-026-38722-1

Ali İhsan Çelik, Ufuk Tunç, Ali Durmuş, Ercan Karaköse, Fatih Özkan Alkurt & Muharrem Karaaslan

We are providing an unedited version of this manuscript to give early access to its findings. Before final publication, the manuscript will undergo further editing. Please note there may be errors present which affect the content, and all legal disclaimers apply.

If this paper is publishing under a Transparent Peer Review model then Peer Review reports will publish with the final article.

ARTICLE IN PRESS

© The Author(s) 2026. **Open Access** This article is licensed under a Creative Commons Attribution-NonCommercial-NoDerivatives 4.0 International License, which permits any non-commercial use, sharing, distribution and reproduction in any medium or format, as long as you give appropriate credit to the original author(s) and the source, provide a link to the Creative Commons licence, and indicate if you modified the licensed material. You do not have permission under this licence to share adapted material derived from this article or parts of it. The images or other third party material in this article are included in the article's Creative Commons licence, unless indicated otherwise in a credit line to the material. If material is not included in the article's Creative Commons licence and your intended use is not permitted by statutory regulation or exceeds the permitted use, you will need to obtain permission directly from the copyright holder. To view a copy of this licence, visit http://creativecommons.org/licenses/by-nc-nd/4.0/.

ARTICLE IN PRESS

Electromagnetic Shielding Performance and Mechanical Properties of Vermiculite-Based Lightweight Geopolymer Mortars

Ali İhsan Çelik*[1] Ufuk Tunç[1], Ali Durmuş[2], Ercan Karaköse[3], Fatih Özkan Alkurt[4], Muharrem Karaaslan[4]

[1]Department of Construction, Tomarza Mustafa Akincioglu Vocational School, Kayseri University, Kayseri, 38940, Turkey

[2]Department of Electrical-Electronics Engineering, Engineering & Architecture and Design Faculty, Kayseri University, Kayseri, 38280, Turkey

[3]Department of Engineering Fundamental Sciences, Faculty of Engineering, Engineering & Architecture and Design Faculty, Kayseri University, Kayseri, 38280, Turkey

[4]Department of Electrical-Electronics Engineering, Faculty of Engineering, Iskenderun Technical University, Iskenderun, Hatay, Turkey

*Corresponding author e-mail address: acelik@kayseri.edu.tr (Ali İhsan Çelik)[1]

ARTICLE IN PRESS

Abstract

In recent years, the widespread use of electronic devices has led to an increase in electromagnetic pollution, which causes electromagnetic interference and reduces the performance of systems. Furthermore, increasing electromagnetic pollution can pose serious risks to human health. This study investigates the development of vermiculite-reinforced lightweight geopolymer composites for protection against electromagnetic pollution. The composites were produced using F-class fly ash and vermiculite in varying proportions between 0% and 100%, along with 10–13 M NaOH solutions. The electromagnetic performance of the 160x140x40 mm tablet samples is evaluated by measuring S_{11}, S_{21}, and shielding effectiveness (SE) for 3-40 GHz frequency bands, 16 GHz and 32 GHz used as representative points for cross-property plots. While electromagnetic SE was characterized across the broad 3–40 GHz band, the frequencies of 16 GHz and 32 GHz are selected as representative points for detailed cross-property analysis and surface plotting to illustrate the interaction between mechanical and electromagnetic performance. All mixtures showed good impedance matching with reflection values below –10 dB. SE results show that V25–M12,

ARTICLE IN PRESS

V50–M12, and V100–M12 mixtures, especially in the Ka band, provided high electromagnetic attenuation by exhibiting resonance peaks above 50 dB. The increase in vermiculite content reduced the bulk density by 8–17% due to its porous structure. Higher molarities (especially 13 M) created a looser microstructure. The highest mechanical flexural strength (8.9 MPa) is obtained with 25% vermiculite and 11 M solution, while the highest compressive strength (30–32 MPa) is obtained with the vermiculite-free control sample. Taguchi analysis showed that the combination of 25% vermiculite and 11–13 M NaOH provided the most balanced mechanical and electromagnetic performance.

Keywords: Vermiculite, Geopolymer, Electromagnetic, Shielding Effect, Alkali Activators

Abbreviations

Electromagnetic Field: EMF
World Health Organization: WHO
Ordinary Portland Cement: OPC
Electromagnetic Shielding: EMS
Electromagnetic Compatibility: EMC
Shielding Effectiveness: SE
Electromagnetic: EM
Electromagnetic Interference: EMI
RADAR CROSS SECTION: RCS
International Agency for Research on Cancer's: IARC
Sodium Silicate: Na_2SiO_3
Sodium Hydroxide: NaOH
Vector Network Analyzer: VNA
The Nicolson-Ross-Weir: NRW
Light Weight Geopolymer Concrete: LWGPC
Field-Scanning Electron Microscopy: FE-SEM
Energy Dispersive X-ray Spectroscopy: EDX
Fourier Transform Infrared Spectroscopy: F-TIR

ARTICLE IN PRESS

Reflection Coefficient: S_{11}
Transmission Coefficient: S_{21}

1. Introduction

The deep penetration of electronic systems into modern infrastructure has made the sustainability of electromagnetic compatibility (EMC) standards a complex engineering problem. Beyond the functional losses in hardware efficiency caused by unwanted emissions, the potential bio-effects of these waves also pose a two-way threat to human health. Therefore, the development of electromagnetic shielding materials with superior attenuation capacity is a scientific necessity in order to minimize these multidimensional risks [1]. This study examines the protective performance and functional effects of vermiculite-modified geopolymer composites in the context of combating electromagnetic pollution. In particular, the potential pathological effects triggered by chronic exposure to electromagnetic fields (EMF) have become the focus of current epidemiological studies. In this context, the International Agency for Research on Cancer's (IARC) classification of low-frequency EMFs as “Group 2B: Possibly Carcinogenic to Humans” reinforces the risks of these fields to biosafety on a scientific level [2]. In parallel, reports published by the World Health Organization comprehensively document the risk-enhancing effects of childhood EMF exposure on the spectrum of leukemia and similar diseases. This correlation, highlighted in the aforementioned reports, scientifically confirms the potential health burden of electromagnetic pollution on pediatric cases [3]. Indeed, studies conducted by Bandara and Carpenter [4] have highlighted that electromagnetic pollution creates a cumulative and severe spectrum of effects on urban infrastructure components. However, despite this contribution to the literature, a scientific gap persists regarding the quantitative analysis of EMF exposure levels in metropolitan areas and the integration of this data into sustainable urbanism models. Therefore, an in-depth investigation of the cross-interactions between site density, infrastructure morphology, and public health dynamics is essential for the construction of energy distribution networks that are compatible with public health.

ARTICLE IN PRESS

High-voltage power transmission lines are among the primary vectors of EMF propagation within the urban fabric. An extensive body of literature provides strong evidence that residing near such infrastructure systems in metropolitan areas increases the incidence of various clinical and pathological complications. This situation confirms, on a scientific level, the need to reassess the location of power transmission lines from a public health perspective [5-8]. The research conducted by Pavlik et al. [9], which focuses on the reflections of EMF on urban morphology, argues that the protective capacity of building components needs to be redefined from both technical and biological perspectives. The authors emphasise that current standards require comprehensive revision, addressing the performance of building materials in response to EMF exposure from both a raw material safety and a bio-health perspective for building occupants. From this perspective, the engineering of innovative building components designed to mitigate electromagnetic pollution is not merely the overcoming of a technical barrier; it has also become a strategic prerequisite for a macro-scale vision of environmental sustainability. In this context, the integration of EMF protection technologies with building materials represents the intersection between ecological security and material functionality in modern urbanism [10-12]. Geopolymers, which offer an ecological and mechanical alternative to traditional Ordinary Portland Cement (OPC)-based construction materials, have risen to a pioneering position in scientific literature thanks to their sustainable synthesis protocols and superior structural resistance. Chemically, these materials represent inorganic polymeric networks obtained through the alkali activation process of aluminosilicate-based precursors. Their ability to incorporate industrial by-products such as fly ash and slag into the circular economy, coupled with their minimized carbon emission profiles, positions geopolymers as a cornerstone of green construction technologies [13-18]. The dual potential of minimizing greenhouse gas emissions and transforming industrial waste into valuable resources makes geopolymers a strategic alternative in ecologically based sustainable construction engineering. The environmental benefits offered by these materials reduce the carbon footprint compared to traditional methods and place circular

ARTICLE IN PRESS

economy principles at the heart of the construction sector [19-23].

Studies conducted by Wang et al [24] have demonstrated that reinforcing geopolymer matrices with components that allow conductivity modulation synchronously enhances both absorption- and reflection-based shielding capacity. In this context, the addition of vermiculite provides a dual-function contribution to the composite structure: on the one hand, it minimizes the structural density of the material, providing a lightweight advantage, while on the other hand, it triggers the internal scattering of electromagnetic waves through the mineral's unique layered morphology, creating a highly effective protective barrier [25-27]. Vermiculite, a natural compound exhibiting a lamellar (layered) structure, possesses high heat resistance and lightness properties. The characteristic porous architecture of this mineral provides advanced capabilities in terms of resistance to heat conduction, as well as deflection and absorption of electromagnetic radiation, giving the material a strategic performance advantage [28-30]. Within the scope of recent experimental studies, the effects of vermiculite substitution and variable sodium hydroxide (NaOH) molarities on the system in fly ash-based geopolymer matrices have been comprehensively analyzed. To determine the characteristic properties of the developed composites, a multidimensional test protocol including thermal conductivity coefficient, water absorption capacity, and mechanical strength parameters was meticulously applied [31]. This has sparked interest in the performance of vermiculite EMS. The study conducted by Selvaraj et al. [32] confirmed that vermiculite modification offers significant absorption performance, particularly in the low-frequency electromagnetic spectrum. The integration of such innovative materials, especially into lightweight structural components, can play a strategic role in attenuating the electromagnetic field intensity associated with uncontrolled urbanization processes and enhancing urban biosecurity [33, 34].

An analytical review of the current academic literature reveals that empirical studies directly focusing on the EMF interaction dynamics of geopolymer-based structural components still represent a significant gap in the literature. The lack of specific research focus on the behaviour characteristics of these alkali-activated matrices in the electromagnetic spectrum indicates that the

ARTICLE IN PRESS

scientific groundwork in this field has not yet fully matured [35-37]. The research conducted by Nguyen et al. [38] detailed the electromagnetic attenuation capacity of geopolymer composites, revealing that the integration of these materials into structural systems offers critical gains in terms of operational and biological safety. The authors establish the scientific basis for the potential of geopolymer matrices to serve as functional EMS in modern building envelopes. The study conducted by Wu et al. [39] meticulously analyzed the EMS performance exhibited by geopolymer variants across different frequency spectra, establishing a predictive model that optimizes material design. Today, the uncontrolled increase in electromagnetic radiation emitted by communication networks and various technological sources constitutes a critical environmental and socio-technical issue for both biological organisms and sensitive electronic instrumentation systems. In this context, 'shielding effectiveness' (SE), defined as the attenuation of electromagnetic energy through reflection and absorption mechanisms, is a parameter directly dependent on the interaction between the wave frequency and the intrinsic electromagnetic characteristics of the protective environment [40].

The integration of vermiculite-based lightweight geopolymer systems into the construction sector offers a functional solution for the attenuation of electromagnetic interference (EMI) and also plays a critical role in minimizing the total carbon footprint of building materials. This dual advantage makes these composites technically and ecologically optimized building components for modern green building standards [41, 42]. The study conducted by Çelik et al. [43] revealed that such material systems offer a strategic contribution to circular economy principles, not only due to their low energy intensity during production stages but also thanks to characteristic features such as recyclability and raw material optimization. The authors highlight the ecological profile of these inorganic polymers, which strengthens the link between resource efficiency and industrial sustainability, emphasizing that they offer a more environmentally friendly production paradigm compared to traditional binders. The study conducted by Maiti et al. [44] quantitatively assessed the environmental impacts of lightweight geopolymer systems,

ARTICLE IN PRESS

revealing that these materials can reduce carbon emissions by 60 per cent compared to traditional cement-based matrices. The authors highlight the alignment of this remarkable emission savings with the decarbonization goals of the construction industry, confirming the strategic role of geopolymers in sustainable building technologies on a scientific level.

Vermiculite, a critical component in the production of structural elements with low specific gravity, demonstrates high utility value across a wide range of fields, from the construction industry to insulation technologies, thanks to its morphological advantages. In this context, the material's balance between lightness and durability acts as a performance catalyst, offering multi-purpose solutions in contemporary building architecture. Although vermiculite has been explored in some electromagnetic applications, its EMS effects have been investigated in a limited number of studies. There are some studies in the literature on the performance of vermiculite in EMS; however, these studies primarily focus on polymer matrix composites. The main originality of the present study lies in the use of vermiculite in geopolymer-bound mortar systems and the evaluation of these systems as a lightweight, environmentally friendly, and cement-free. There is no study in the literature that investigates the EMS performance of vermiculite-added geopolymer mortars, particularly in the EM wave bands and using the free-space vector network analyzer (VNA) measurement method. In this respect, the study clearly differs from existing studies in terms of material type (geopolymer mortar), binder system (cement-free), measurement approach, and frequency range. LWGPC with vermiculite additive can provide protection against EM waves, thereby reducing the potential EM effects on human health and contributing to the construction of sustainable, safe, and energy-efficient living spaces. However, the most important alkali activator component in geopolymer production is obtained by electrolysis of NaOH. In the study, the effect of vermiculite additive as well as NaOH molarity is tested on the samples produced. For this purpose, the geopolymer mixtures used in the study are composed of fly ash, sodium silicate (Na_2SiO_3), NaOH, and varying proportions of vermiculite. A total of sixteen distinct mixtures are prepared, in which the vermiculite content is systematically increased to 0%, 25%, 50%, and 100%, while the

ARTICLE IN PRESS

sand content is proportionally reduced. The molarity of the NaOH solution is adjusted between 10 M - 13 M. Through this design, both the mechanical strength and the potential EMS capability of the composites are evaluated. The development of vermiculite-reinforced geopolymer structural elements is expected to provide an innovative solution for protecting human health in urban environments while simultaneously supporting environmental sustainability goals [45-47]. It is anticipated that the findings from this research will create new scientific momentum at the intersection of electromagnetic spectrum management, advanced material architecture, and sustainable urban planning strategies. This study aims to serve as a catalyst for interdisciplinary work towards multidimensional and integrated engineering solutions by dissolving the conceptual boundaries between the specified disciplines.

2. Material Method

2.1. Mixture Composition and Sample Preparation

The geopolymer mortar samples utilized in this study are produced using mixtures containing 100% F class fly ash as the primary binder and expanded vermiculite at varying proportions. Na_2SiO_3 and NaOH solutions are employed as alkali activators. Na_2SiO_3 is selected at 50 °Bé and 2 modulus values. The NaOH solution is prepared at four different molarities (10M, 11M, 12M, and 13M), while the Na_2SiO_3/NaOH ratio is maintained constant across all mixtures. Maintaining the Na_2SiO_3/NaOH ratio at 1.5 is based on the fact that this ratio is widely accepted in geopolymer chemistry and has been reported in many previous studies to provide optimal mechanical performance and a balanced Si/Al ratio. By keeping this ratio constant, the variable effects of the alkali activator composition are minimized, and the effects of NaOH molarity and vermiculite substitution ratios, which are the main focus of the study, can be more clearly revealed. The primary reason for selecting a NaOH molarity in the range of 10–13 M is that the literature reports that effective dissolution and polymerization reactions in aluminosilicate-based geopolymer systems generally occur with maximum efficiency within this range. At lower molarities (≤8 M), it

ARTICLE IN PRESS

is commonly reported that aluminosilicate dissolution is insufficient, resulting in low reaction rates and poor mechanical performance. Conversely, at molarities of 14 M and above, excessive alkalinity is known to negatively affect mechanical properties by causing rapid precipitation, irregular gel formation, increased shrinkage, and microcrack development. Additionally, the reduced workability and impracticality of very high molarities from a safety perspective have also influenced the determination of the upper limit of this range.

The fly ash content is kept consistent, and vermiculite is incorporated at volumetric ratios of 0%, 25%, 50%, and 100%, determined in accordance with Rilem sand standards. Correspondingly, the quantity of sand is reduced to maintain a constant total aggregate volume. To establish a systematic parametric analysis, vermiculite replacement ratios were set at 0%, 25%, 50% and 100% on a volumetric basis. The 0% substitution level, functioning as the control group, provided the basic reference values; the intermediate levels of 25% and 50% were included in the experimental set to determine the gradual interaction of the mineral at the binder-filler interface and the possible optimum performance threshold. Despite causing a radical decrease in mechanical strength values, the 100% substitution ratio was deliberately selected as a “limit value” variable to empirically define the behavioural limits of the matrix, its performance capacity under extreme conditions, and the operational limits of the material.

Adhering to the design matrix detailed in Table 1, a total of sixteen different compositions were formulated. In all experimental variations, chemical activation was achieved by using 305.18 Kg of Na_2SiO_3 and 203.29 kg of NaOH solution, in addition to a binder content fixed at 766.28 kg/m³. In all mixtures, the Na_2SiO_3/NaOH ratio was stabilized at a level of 1.5 to achieve methodological consistency. The components were mixed using fixed-speed mechanical mixers until complete homogenization between phases was achieved; the freshly prepared mortars were then poured into moulds and subjected to a systematic curing and performance testing protocol.

ARTICLE IN PRESS

Table 1. Experimental mix design

S.No	Mix. Code	Fly Ash	Na_2sio_3	NaOH	NaOH Molarity	Vermiculite	Sand (Rilem)	Rate of Vermiculite
		kg/m³	**kg/m³**	**kg/m³**	**M**	**kg/m³**	**kg/m³**	**%**
1	V0-M10	766.28	305.18	203.29	10	0.00	957.85	0
2	V0-M11	766.28	305.18	203.29	11	0.00	957.85	0
3	V0-M12	766.28	305.18	203.29	12	0.00	957.85	0
4	V0-M13	766.28	305.18	203.29	13	0.00	957.85	0
5	V25-M10	766.28	305.18	203.29	10	30.60	722.45	25%
6	V25-M11	766.28	305.18	203.29	11	30.60	722.45	25%
7	V25-M12	766.28	305.18	203.29	12	30.60	722.45	25%
8	V25-M13	766.28	305.18	203.29	13	30.60	722.45	25%
9	V50-M10	766.28	305.18	203.29	10	61.20	361.23	50%
10	V50-M11	766.28	305.18	203.29	11	61.20	361.23	50%
11	V50-M12	766.28	305.18	203.29	12	61.20	361.23	50%
12	V50-M13	766.28	305.18	203.29	13	61.20	383.14	50%
13	V100-M10	766.28	305.18	203.29	10	122.40	0.00	100%
14	V100-M11	766.28	305.18	203.29	11	122.40	0.00	100%
15	V100-M12	766.28	305.18	203.29	12	122.40	0.00	100%
16	V100-M13	766.28	305.18	203.29	13	122.40	0.00	100%

ARTICLE IN PRESS

ARTICLE IN PRESS

In this study, fly ash, used as the primary precursor material in the geopolymerisation process, was sourced from the Zonguldak Thermal Power Plant and incorporated into the experimental process. When the chemical spectrum of the raw material was examined as detailed in Table 2 the cumulative concentration of the SiO_2, Al_2O_3, and Fe_2O_3 components exceeded the cumulative concentration threshold of 70%, while the CaO content remained below the 10% limit. This oxide composition is fully consistent with the characteristic parameters that enable the fly ash used to be classified as Class F under ASTM C618 standards [48, 49]. Vermiculite is a group of minerals that exhibits significant volumetric expansion when subjected to thermal processing and displays a characteristic decomposition behaviour known as “exfoliation” (flaking) during this process due to its layered morphology. Derived etymologically from the Latin word vermiculare (worm-like curling), this term describes the unique macro-structural form change exhibited by the mineral under the influence of heat. Intrinsically low in density, with high thermal stability and non-combustible properties, this mineral is considered a strategic additive in critical areas of modern construction technology, such as acoustic/thermal insulation, passive fire protection and lightweight composite production.

Expanded vermiculite, thanks to its micro-porosity, offers high heat resistance and is therefore the preferred choice in fire-resistant plaster formulations, insulation mortars and lightweight concrete designs. Furthermore, the mineral's high water adsorption capacity improves the rheological properties of fresh concrete and allows for control of setting times. All these technical qualities position vermiculite as an indispensable performance component in the development of sustainable and energy-efficient building components [50]. The elemental composition and oxide distributions of all binding components used have been meticulously characterized using X-ray fluorescence (XRF) spectrometry. The comprehensive data obtained from this spectroscopic analysis are detailed in Table 2, reflecting the chemical profile and purity levels of the materials.

Table 2. Chemical components and percentages of binders

ARTICLE IN PRESS

Components	Fly Ash	Vermiculite
$CaCO_3$ (%)	-	-
$MgCO_3$ (%)	-	-
CaO (%)	1.87	2-4
SiO_2 (%)	59.2	38-39
Al_2O_3 (%)	20.3	15-16
Fe_2O_3 (%)	7.65	11-13
Cr_2O_3(%)	-	0.01-0.05
P_2O_3 (%)	-	0.02-0.08
SO_3 (%)	0.19	0.05-0.1
MgO(%)	2.21	15-16
MnO(%)	-	0.1-0.15
Na_2O(%)	1.56	0.2-0.3
K_2O (%)	2.36	5-6
BaO(%)	-	0.5-0.7
TiO(%)	-	2-3
SrO(%)	-	0.25
Loss of Fire (%)	3.23	-
Specific Gravity(g/cm^3)	2.35	0,06 – 0,15
Particle size(mm)	0,01 – 0,03	05-3

ARTICLE IN PRESS

To evaluate the mechanical properties, cube specimens measuring 40x40x40 mm and prism specimens measuring 40x40x160 mm are prepared for compressive and flexural strength tests, respectively. Rectangular prism molds with dimensions of 160x140x40 mm are utilized for electromagnetic testing. After casting, all samples are left in the molds for an initial setting period and subsequently subjected to heat curing at 85 °C for 24 hours. Following the heat treatment, the specimens are conditioned at room temperature in a stable environment, and the relevant tests are conducted under these conditions. A schematic representation of the experimental procedure, the different specimen types, and the intended purpose of each specimen is provided in Fig. 1.

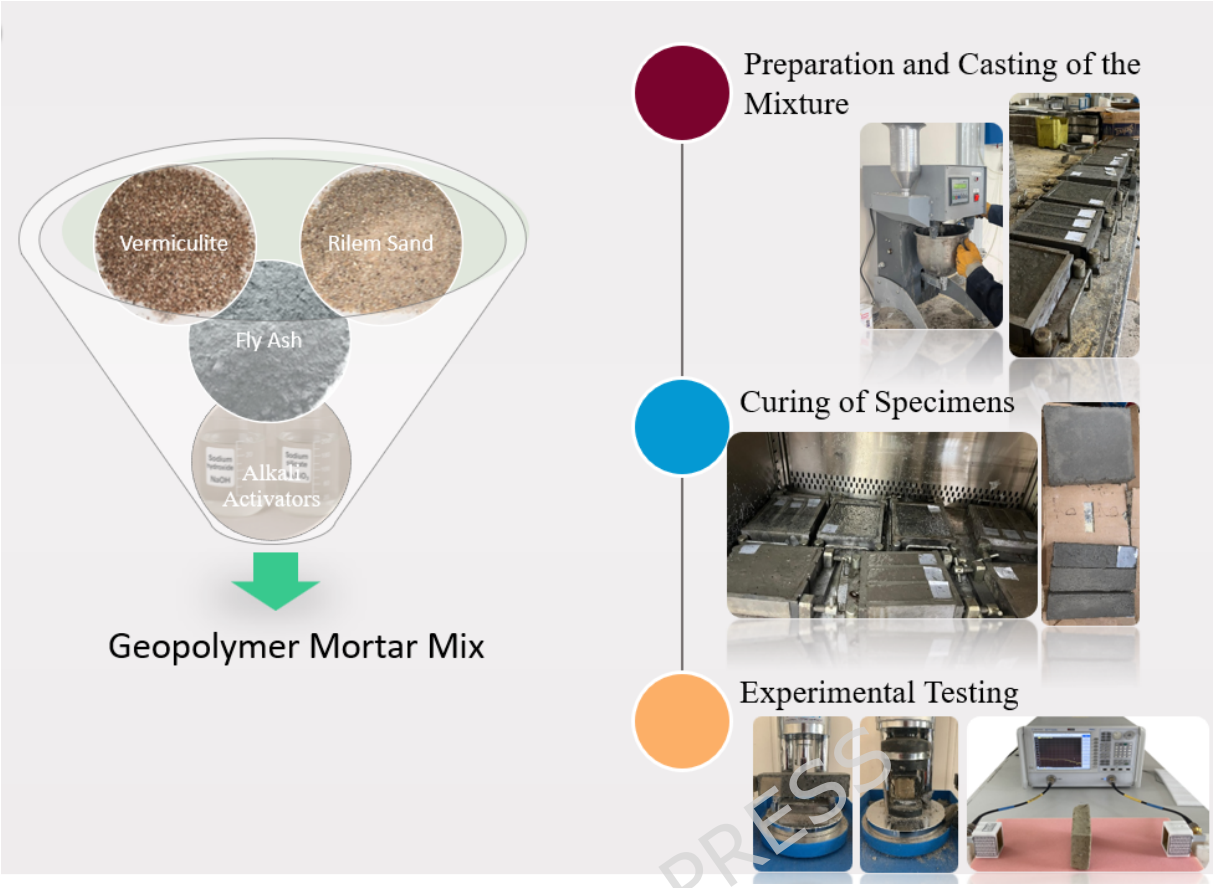


Fig. 1. Flow Chart of production and tests

ARTICLE IN PRESS

2.2. Designing the Test Setup for Electromagnetic (EM) Tests

To empirically validate the EMS capacity of LWGPC samples, an original experimental configuration, detailed in Fig. 2, was devised. The primary function of this setup is to quantify the absorption, reflection, and transmission characteristics of the samples within a specific frequency spectrum with high precision. The methodological framework adopted in this regard is based on the integration of a VNA with high-gain horn antennas and is built upon the principles of the 'Free-Space Method', which is accepted in the literature as a standard approach for material characterization [51, 52]. In determining the effectiveness of EMS, the ASTM D4935–18 protocol [53], which is internationally recognized as the technical authority for characterizing planar samples, was used as a

ARTICLE IN PRESS

reference. Measurements conducted in accordance with this standard ensured the comparability and methodological validity of the data obtained, enabling the analysis of material performance on a standardized plane.

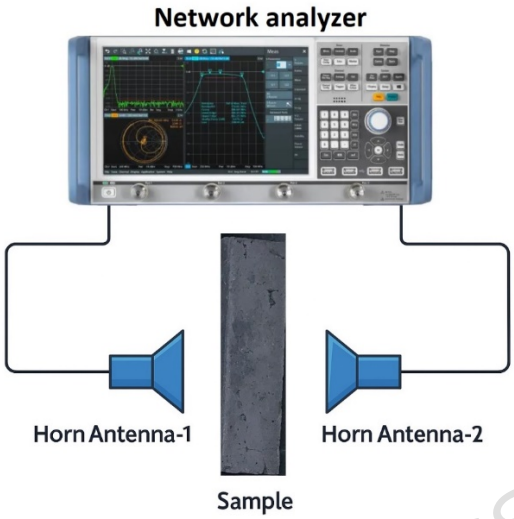


Fig. 2. Schematic Representation of the Electromagnetic Measurement Setup

ARTICLE IN PRESS

The experimental architecture schematized in Fig. 3 consists of two horn antenna configurations positioned opposite each other on either side of the sample; one of these units performs signal transmission (Transmitter - Horn Antenna-1), while the other performs signal reception (Receiver - Horn Antenna-2). These antennas are specially designed to ensure operational continuity across a wide frequency spectrum and to precisely maintain the directivity of electromagnetic wave propagation. Both antenna units are integrated with a VNA to manage the data collection process. The test sample is strategically positioned perpendicular to the antennas' focal center and electromagnetic wave path. The primary propagation parameters quantified in this measurement protocol are the S_{11} and S_{21} coefficients, representing the ratios of energy reflected from and transmitted through the sample, respectively.

$$S_{11}=\frac{E_{ref}}{E_{inc}} \quad (1)$$

$$S_{21}=\frac{E_{trans}}{E_{inc}} \quad (2)$$

ARTICLE IN PRESS

where E_{inc}, E_{ref}, and E_{trans} represent the amplitudes of the incident, reflected, and transmitted electromagnetic waves, respectively, these parameters are directly measured using a VNA and recorded in a digital environment. For the calculation of SE, these parameters are converted to logarithmic units (dB) as follows:

$$S_{11}(dB) = 20\log_{10}(|S_{11}|) \quad (3)$$

$$S_{21}(dB) = 20\log_{10}(|S_{21}|) \quad (4)$$

The cumulative screening performance of composite samples represents the total attenuation in transmitted power due to the synergistic effect of reflection and absorption mechanisms. This value is obtained as an analytical function of the difference between the free space reference measurement and the measurement data in the presence of the sample. Defined as the attenuation capacity of electromagnetic waves on the propagated energy, SE was calculated in this study according to the $20\log_{10}$ rule, which expresses the power loss on a logarithmic scale, based on the electric field amplitude ratios determined by the VNA. The numerical breakdown of the total SE values is determined by differentially comparing the signal strength passing through the concrete-based sample with the reference free-space transmission characteristics, as detailed in Eq. (5):

$$SE\ (dB) = 20\log_{10}\left(\frac{|S_{21,free}|}{|S_{21,sample}|}\right) = S_{(21,free)(dB)} - S_{(21,sample)(dB)} \quad (5)$$

Considering the electromagnetic characteristics of the lossy and high porosity geopolymer matrices examined in this study, the transmission-based total SE has been accepted as a performance indicator that is both theoretically sufficient and decisive in terms of engineering applications,

ARTICLE IN PRESS

reflecting the material's energy attenuation capacity. Particularly considering the energy dispersion caused by multiple internal reflections in porous structures and lossy matrix components, this cumulative value obtained from transmission data constitutes the most practical and reliable parameter validating the material's real-world protection potential. This approach is justified by the fact that in electrically thick (40 mm) cementitious composites, absorption typically serves as the primary shielding mechanism, and the effects of multiple internal reflections are significantly dissipated within the heterogeneous microstructure.

For the lossy and porous vermiculite-based geopolymer composites analyzed here, the transmission-based total SE is a sufficient and practically relevant metric. Given the 40 mm specimen thickness, electromagnetic energy is primarily dissipated through internal absorption and multiple scattering paths within the heterogeneous microstructure, making absorption the dominant shielding mechanism.

2.3. Free-Space Microwave Measurements for 3-40 GHz Frequency Region

Free-space microwave measurements are carried out to characterize the electromagnetic response of 16 different LWGPC samples across the 3–40 GHz frequency range. The actual measurements are carried out using a free-space transmission method with horn antennas and a vector network analyzer, which is a widely accepted approach for broadband and high-frequency shielding characterization. The free space setup enables plane wave illumination and avoids the geometric and frequency limitations associated with coaxial fixtures. Each sample had dimensions of 16 cm × 16 cm with a uniform thickness of 4 cm. Two distinct measurement setups are employed using a Keysight PNA-L vector network analyzer, which supports measurements up to 43.5 GHz.

As detailed in Fig. 3(a), the first experimental configuration consists of a two-port measurement system covering the 3–18 GHz frequency spectrum via broadband horn antennas integrated into the VNA ports. The second setup, dedicated to high-frequency characterization (Fig. 3(b)), uses horn

ARTICLE IN PRESS

antenna variants operating in the 15–40 GHz band with a similar architecture. In both systems, the antenna units are positioned face-to-face at a fixed distance of 50 cm; the test specimens are placed at the exact center of the signal propagation path, equidistant from the antennas. Prior to the data acquisition phase, a full two-port calibration was performed using the standard Short-Open-Load-Transition (SOLT) calibration protocol to ensure the accuracy and precision of the scattering parameters. The complex scattering parameters (S_{11} and $S_{21)}$ are recorded to characterize the reflection and transmission characteristics of each sample across the measured spectrum. These parameters are converted to decibels (dB) using the Eq. 3 and Eq. 4, which express the reflected and transmitted power ratios on a logarithmic scale:

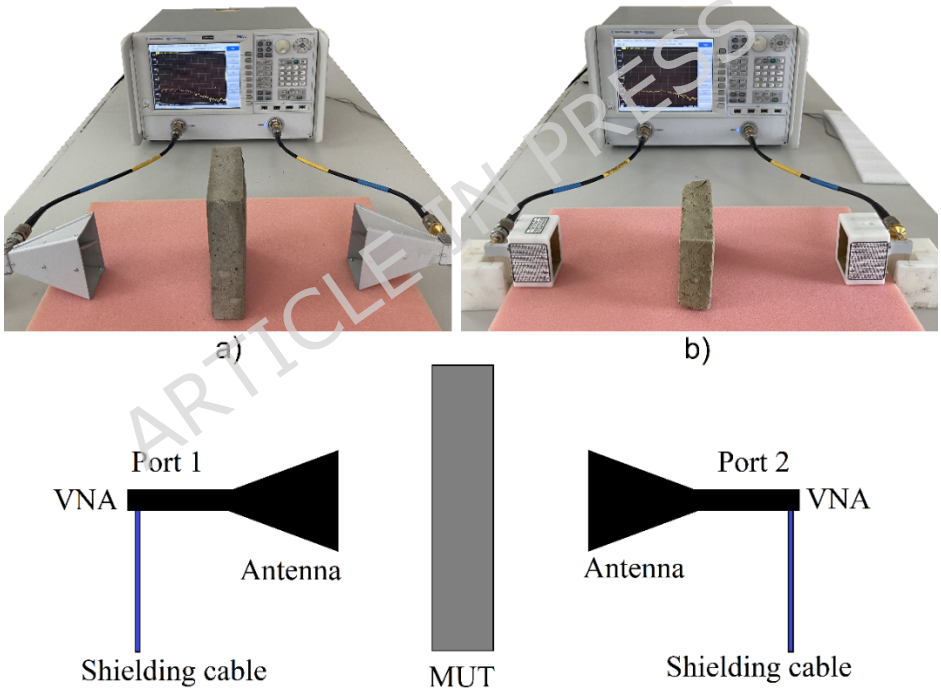


Fig. 3. Free-space measurements for **a)** 3-18 GHz and **b)** 15-40 GHz

2.4. Mechanical tests

To ensure the statistical reliability and reproducibility of the experimental results, three specimens were prepared for each mix composition. These specimens were then subjected to a comprehensive characterization procedure encompassing both mechanical

ARTICLE IN PRESS

performance parameters and EMS-related characteristics. Accordingly, the compressive strength properties of the specimens were evaluated in accordance with ASTM C109/C109M [54], quantified in accordance with the ASTM C109/C109M protocol, while flexural strength analyses were meticulously conducted based on the technical criteria defined in ASTM C348 [55]. The experimental configuration and test instrumentation used for the bending and compressive strength tests applied as part of the mechanical characterization of the samples are presented in detail in Fig. 4. This setup, detailed in the Fig., represents the technical infrastructure that validates the compliance of critical parameters such as loading speed and sample positioning with standards

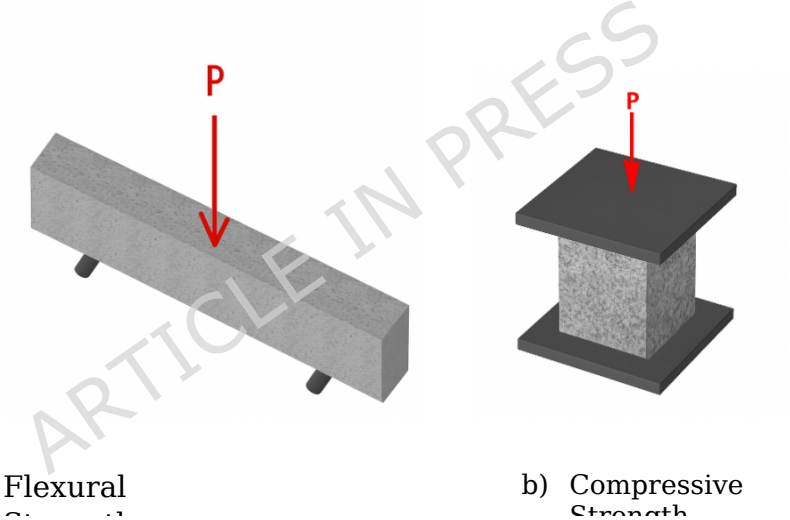


Fig. 4. Experimental setups and instrumentation details used in the mechanical characterization process

Data obtained from EMS measurements were integrated with the samples' compressive and flexural strength values to create a comprehensive performance matrix. In this analytical process, the decisive role of variable vermiculite substitution ratios and NaOH molarity levels on material characteristics was examined from a multidimensional and comparative perspective. Thus, the correlation between parametric changes in the mixture design and both functional (electromagnetic) and structural (mechanical) properties has been systematically revealed.

ARTICLE IN PRESS

3. Result and Discussion

3.1 Electromagnetic Resistance

In the experimental process covering the 3-18 GHz frequency spectrum, a total of 17 different measurements were performed, consisting of a reference measurement without a sample (free space baseline) and 16 consecutive sequences conducted for each LWGPC variant. This empirical data set allows for a comparative and in-depth analysis of the electromagnetic interaction established by each composite matrix with the incident microwave radiation. When examining the data presented in Fig. 5, it can be seen that the S_{11} reflection coefficient profiles exhibit remarkable spectral stability across the entire bandwidth. The smooth and consistent S_{11} profile provided by the reference measurement definitively confirms that there is no impedance mismatch or environmental clutter in the test setup. The S_{11} behavior observed for all LWGPC samples follows a stable trend, free from resonance distortion or scattering-induced anomalies. This proves that the samples do not exhibit critical back reflections in the direction of the transmitter antenna (Port 1), confirming the methodological robustness of the free-field configuration and antenna alignment. This high stability in the S_{11} data also validates the effectiveness of the applied two-port calibration and the system reliability across the wide bandwidth.

ARTICLE IN PRESS

The absence of distinct resonance peaks or standing wave patterns in the measured spectrum confirms that the antenna spacing and sample positioning have been optimized to minimize multiple reflections and establish far-field conditions. Although the sixteen different LWGPC variants presented in Fig. 5 exhibit a similar reflection coefficient trend across the 3–18 GHz frequency band, they display unique spectral signatures in specific sub-bands due to their intrinsic absorption characteristics. Specifically, the V0-M10, V0-M12, V50-M13, and V100-M12 compositions indicate strong electromagnetic attenuation potential, exhibiting sharp minimum values reaching 30 dB and −40 dB levels in the

ARTICLE IN PRESS

8–10 GHz range. On the other hand, the V25-M12 and V25-M13 samples stand out for broadband absorption applications by offering balanced attenuation performance across a broader spectrum of 8–14 GHz. Comparatively, the relatively high reflection tendency of the V0-M11, V0-M13, and V100-M10 mixtures in the low-frequency region suggests that a reflection-based response dominates over the absorption mechanism in this region. V25-M10, V50-M11, and V50-M12 are characterized by resonance behaviors that become pronounced in the mid-to-high frequency bands 10–14 GHz). In general, these variations observed between samples can be attributed to the modifications of mineral additives and activator molarity on the relative permeability (ε_r) and dielectric loss factor of concrete. In light of these data, the V0-M12, V25-M12, V50-M13, and V100-M12 mixtures are considered the most promising candidates for advanced EMS and wave absorption technologies.

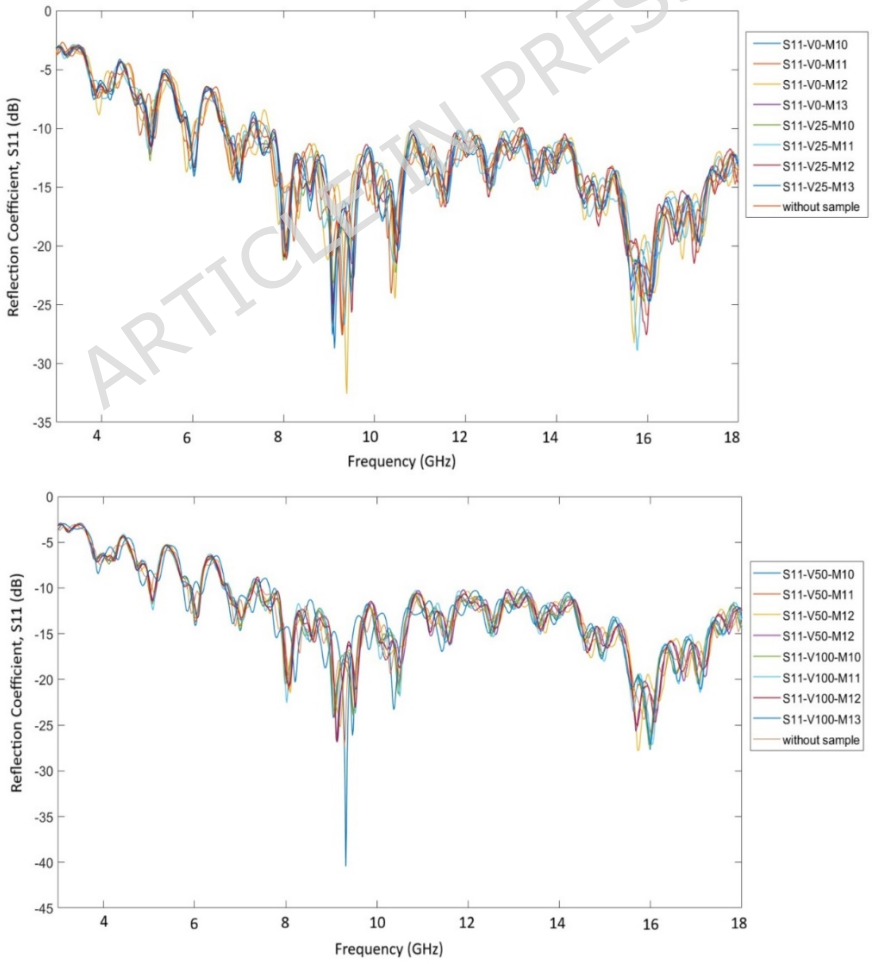


Fig. 5. 3-18GHz Reflection Coefficient (S_{11}) results in dB

ARTICLE IN PRESS

Fig. 6 details the transmission coefficient (S_{21}) profiles of concrete specimens coded V0-M10 to V100-M13in the 3-18 GHz frequency spectrum. Experimental findings reveal that all LWGPC variants exhibit varying levels of transmission loss compared to the free space (air) reference value; this validates the absorption-based energy losses occurring during the passage of electromagnetic waves through the matrix. Compared to the reference line without a sample, a radical decrease in transmitted signal strength was detected in all samples, proving that the wave was subjected to effective attenuation throughout the material thickness. Within the data set in Fig. 6(a), the V0-M11 and V25-M11 samples stand out with their superior performance. Specifically, the V0-M11 mixture creates deep attenuation valleys reaching V0-M11 dB levels in the 8–16 GHz band, while 50 dB. V25-M11 exhibits a broader bandwidth and a noteworthy spectral response. Other samples V0-M10, V0-M12, V0-M13, V25-M10, V25-M12, V25-M13) generally exhibit a moderate attenuation capacity ranging from 20 to −35 dB. Based on these data, it has been concluded that the V0-M11 and V25-M11 compositions are strategic candidates for high-performance EMS applications.

As detailed in Fig. 6(b), within the V50-M10–V100-M13 series; the V50-M11, V50-M13, V100-M12 and V100-M13 compositions exhibited the most noteworthy spectral responses. In particular, the V50-M11 sample stood out as the most effective variant in the test set, demonstrating superior performance with extreme attenuation values reaching 70 dB levels in the 14–18 GHz band. Similarly, the V50-M13 and V100-M12samples also remained below the -50 dB threshold, confirming a strong absorption capacity in the high-frequency spectrum. Comparatively, the V50-M10, V50-M12, V100-M10, and V100-M11 variants exhibited a more stable and moderate attenuation ranging from 25 to 35 dB. When the obtained data are examined from a holistic perspective, both experimental groups exhibit significant inter-sample performance variation. Specifically, the compositions V0-M11, V25-M11, V50-M11, V50-M13, V100-M12, and V100-M13 compositions stand out as the most effective formulations for damping electromagnetic radiation transmission. These findings validate

ARTICLE IN PRESS

that electromagnetic modifications induced by functional additives play a critical role in matrix characterization particularly at high frequencies and that concrete can be engineered as a high-tech shielding medium through appropriate component selection. Furthermore, the results demonstrate that specific concrete formulations can function as 'moderate absorber' materials capable of absorbing the microwave spectrum without producing destructive secondary reflections. This technical capability is a vital performance parameter for strategic application areas such as electromagnetic interference (EMI) protection, radar cross section (RCS) minimization, and urban microwave propagation modeling

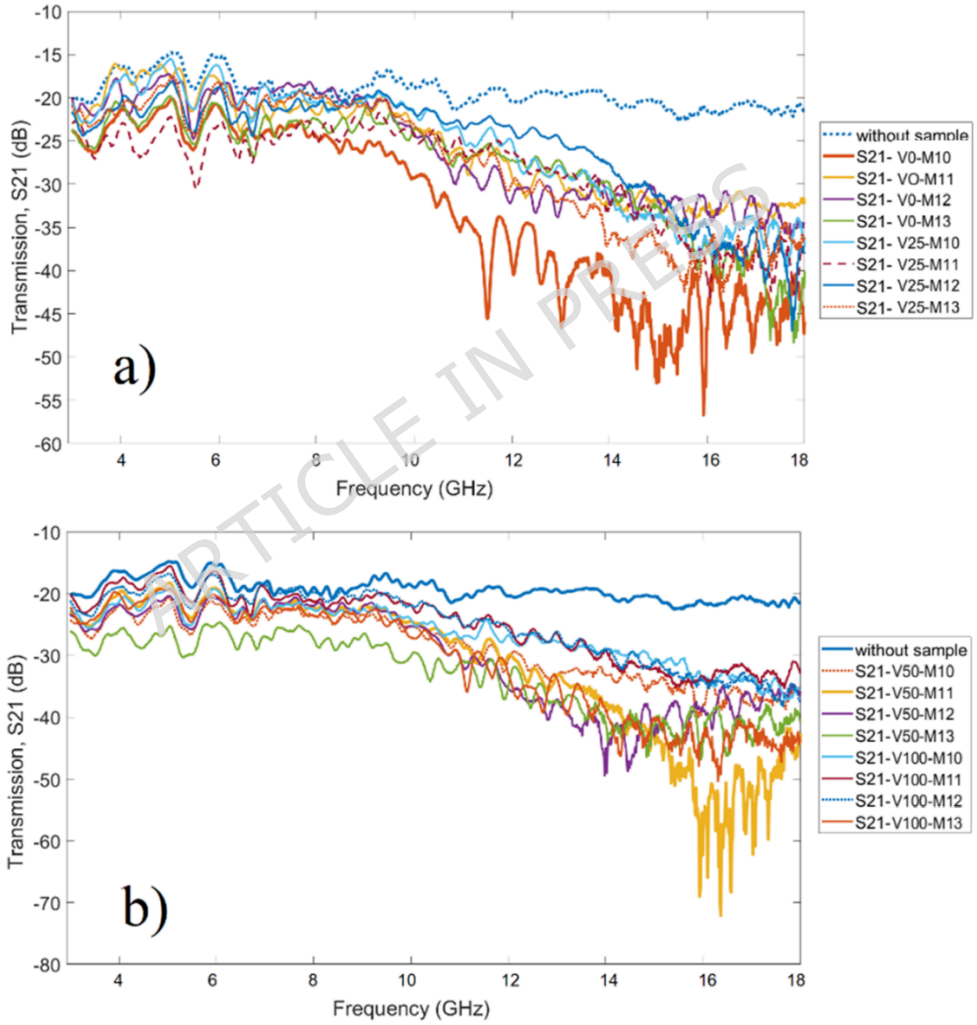


Fig. 6. Transmission Coefficient (S_{21}) results in dB at 3-18GHz measurements **a)** for V0-M10 to V25-M13 and **b)** for V50-M10 to V100-M13

In high-frequency characterization studies covering the 15–40 GHz band, the S_{11} parameter was subjected to a systematic analysis for sixteen

ARTICLE IN PRESS

LWGPC samples and the free-space reference condition. In light of the data presented in Fig. 7, it is seen that the reflection characteristics generally exhibit a linear and stable profile throughout the measured spectrum. In these comparatively conducted measurements, all spectral traces generally reveal reflection coefficients below the 10 dB threshold, indicating broadband and acceptable impedance matching. In particular, a distinct resonance phenomenon was observed around 30 GHz, where the return loss decreased to levels between 40 to 45 dB; this confirms that the system achieved strong impedance matching at the relevant frequency. Additionally, a secondary attenuation region was detected in the 36–38 GHz band.

Following the inclusion of the samples in the test setup, the precise shifts detected in the spectral positions and amplitudes of the resonance minima; intrinsic electromagnetic parameters such as relative permittivity and dielectric loss tangent clearly demonstrate how intrinsic electromagnetic parameters modulate the impedance matching conditions of the system. The overall data set demonstrates a high level of metrological fidelity, confirming the reproducibility of the experiment; it also offers sufficient sensitivity to capture controlled yet distinguishable nuances between samples. This definitively validates the analytical sensitivity and methodological validity of the measurement configuration against microscopic variations in dielectric properties and changes in sample placement.

ARTICLE IN PRESS

ARTICLE IN PRESS

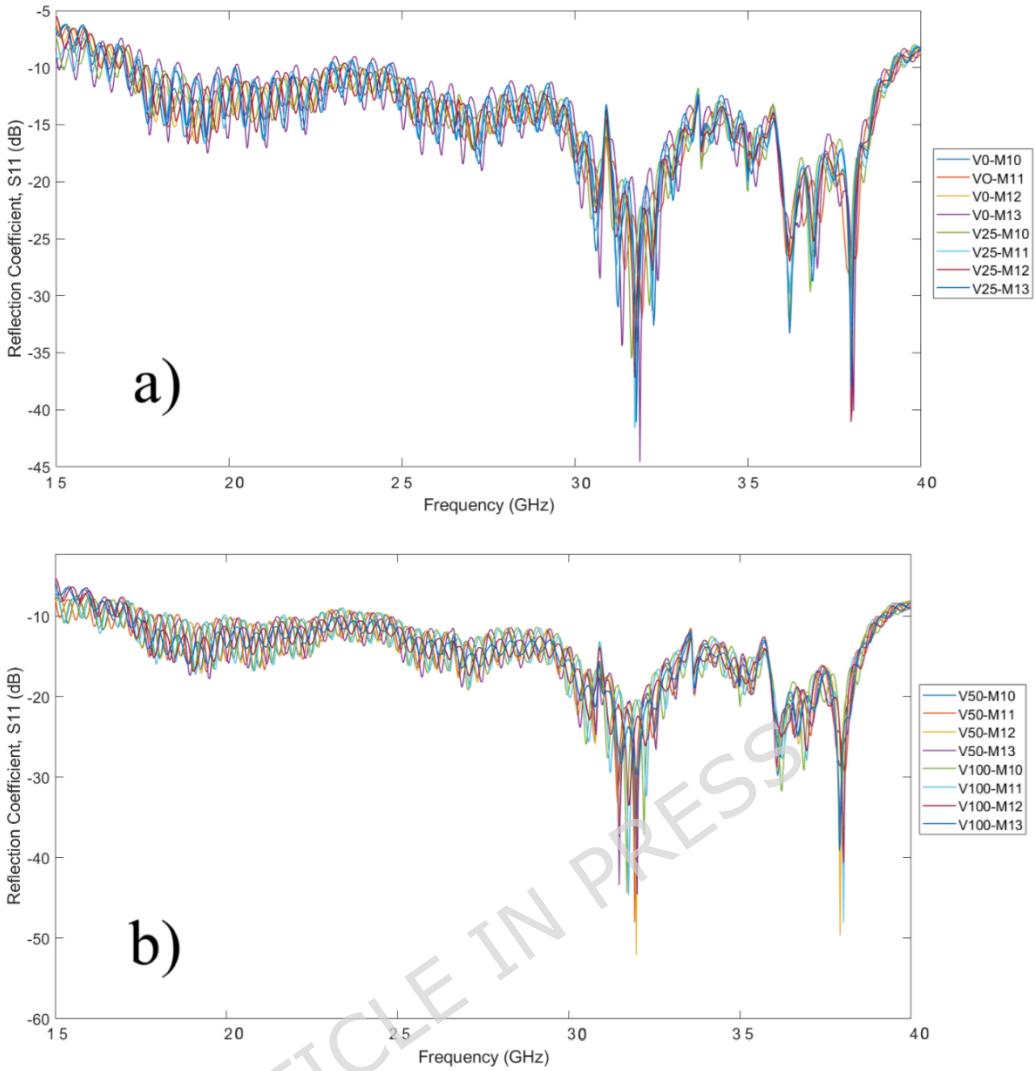
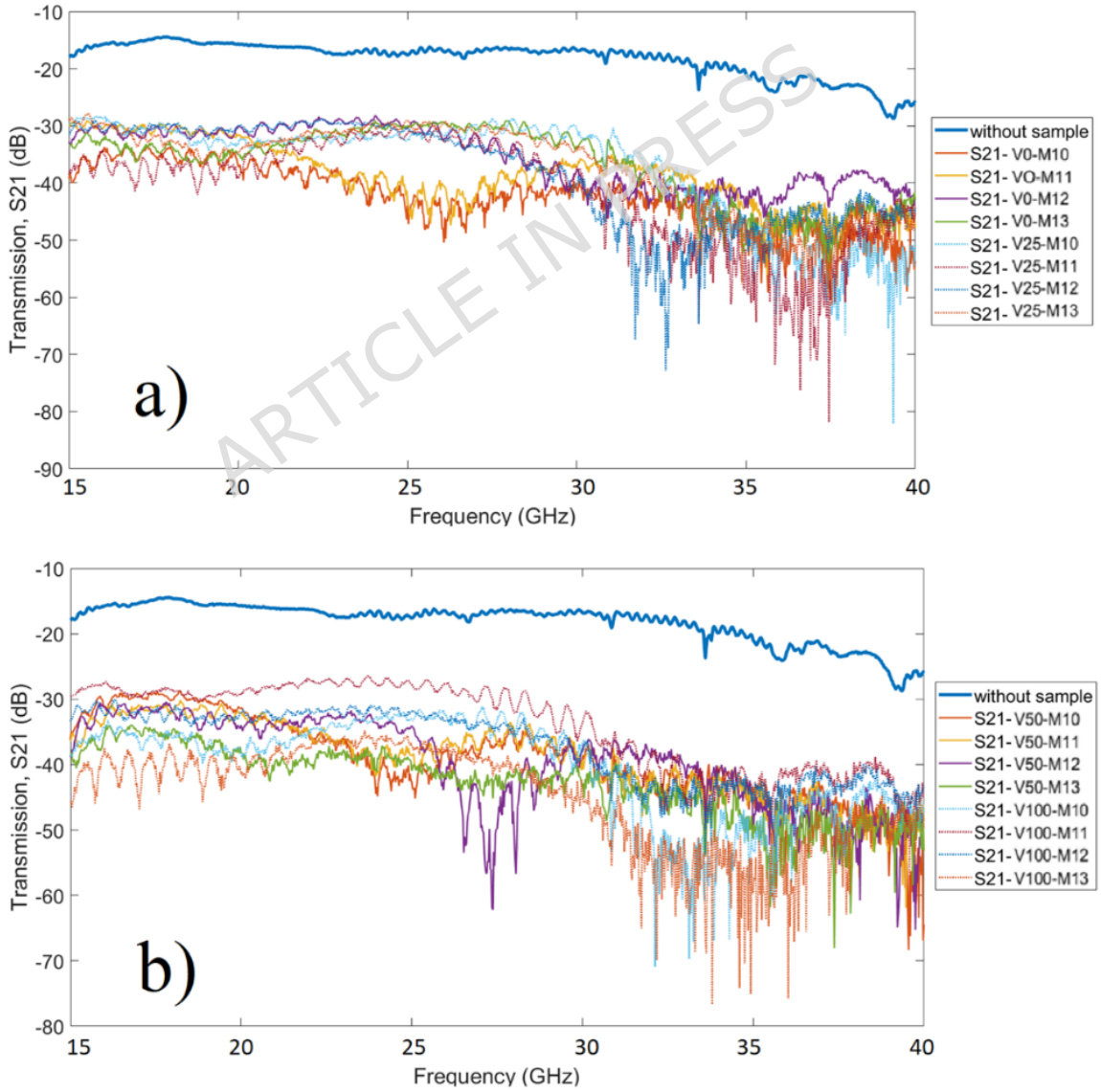


Fig. 7. 15-40 GHz Reflection Coefficient (S_{11}) results in dB

Fig. 8 presents the transmission coefficient (15-40) spectra of concrete specimens from the V0-M10 to V100-M13 series in the 15-40 GHz millimeter-wave regime on a decibel (dB) scale. Fig. 8(a) summarizes the findings for the V0-M10 to V100-M13. groups, while Fig. 8 (b) analyzes the V0-M10 to V25-M13 variants comparatively with the free space reference. In both cases, the reference line without the sample exhibits relatively high transmission in the 15 to 20 dB band, while the inclusion of the test sample causes a radical drop in the S_{21} values. In the presence of the sample, an additional attenuation of 10–30 dB was detected across the entire band, and it was observed that transmission losses deepened with increasing frequency. The transmission levels of some samples falling below the 60 dB threshold in the 25–40 GHz range indicate an extremely strong

ARTICLE IN PRESS

electromagnetic absorption capacity. Both data sets reveal significant variation between samples in terms of dielectric properties, density, spectral ripples arising from microstructural differences, and loss magnitude. Furthermore, the sharp drops observed in the transmission curves, particularly in the resonance regions of the 30–35 GHz band, symbolize the activation of high loss mechanisms in wave-material interaction and prove the characterization accuracy of the setup at these critical frequencies. Cumulatively, the S_{21} results confirm that the platform can reliably distinguish materials based on their conductivity and absorption capabilities across a wide bandwidth, supporting its use in advanced sensing and characterization applications.



ARTICLE IN PRESS

Fig. 8. Transmission Coefficient (S_{21}) results in dB at 15-40GHz measurements **a)** for V0-M10 to V25-M13 and **b)** for V50-M10 to V100-M13

3.2. Free-Space Microwave Shielding Calculations by Measurement Results

SE quantifies the ability of a material to attenuate electromagnetic waves, and is commonly expressed in dB. It represents the reduction in transmitted power due to reflection, absorption, and multiple internal reflections within the material. In this study, SE is determined by comparing the transmitted signal power through concrete samples with that of a reference free-space condition. The SE is calculated as the difference between the free-space and sample S_{21} magnitudes in dB, following the relation $SE(f)=S_{21free}(f)-S_{21sample}(f)$. This adopted methodological framework enables the frequency-dependent spectral analysis of electromagnetic SE by quantifying the cumulative attenuation responses induced by composite matrices. The high SE values obtained represent superior efficiency in the attenuation of incoming microwave radiation; these data constitute a decisive performance criterion for strategic engineering disciplines such EMC, interference management, and stealth technologies.

Fig. 9 details the SE characteristics of 16 different concrete compositions tested in the 3–18 GHz frequency spectrum. In this context, Fig. 9 (a) presents the V0-M10 to V25-M13 and V50-M10 to V10-M13 series, while Fig. 9(b) presents the V50-M10 to V10-M13 variants in a comparative manner. Empirical findings reveal a frequency-sensitive protection profile for each sample, reflecting a correlation where SE values gradually increase towards the upper limit of the spectrum. When examining the general spectral trend, it is observed that all samples exhibit nominal shielding in the low-frequency regime 3–8 GHz), ranging from 0–10 dB. However, once the 10 GHz threshold is exceeded, the attenuation performance accelerates, reaching levels of 30–50 dB in the high-frequency band. Specifically for the samples in the first group, the V0-M10

ARTICLE IN PRESS

and V25-M10 compositions exhibited dominant performance in the 12–18 GHz range; in particular, the V0-M10 sample stood out by recording peak values of approximately 35–40 dB. In contrast, the V0-M11, V0-M13, and V25-M12 samples exhibit spectrally more linear but relatively limited performance improvements. When examining the second group of data presented in Fig. 9(b), it is seen that the V0-M10 composition achieves values of 45–50 dB in the 14–18 GHz band, validating the highest SE among all samples. These findings clearly demonstrate the decisive role of material composition and structural parameters on the sample groups. While the shielding response in the first series V0-M10–V25-M13 follows a stable and moderate trend, certain variants in the second group particularly offer a much stronger EMI attenuation capacity at high frequencies due to the synergistic interaction between absorption and reflection mechanisms. In this context, the study quantitatively demonstrates the broadband protection potential of different formulations and identifies critical candidates for millimeter-wave applications. Ultimately, the results confirm the potential of specific concrete formulations for use as functional EMS materials, highlighting the strong dependence of SE performance on both the frequency regime and sample-specific characteristics.

ARTICLE IN PRESS

ARTICLE IN PRESS

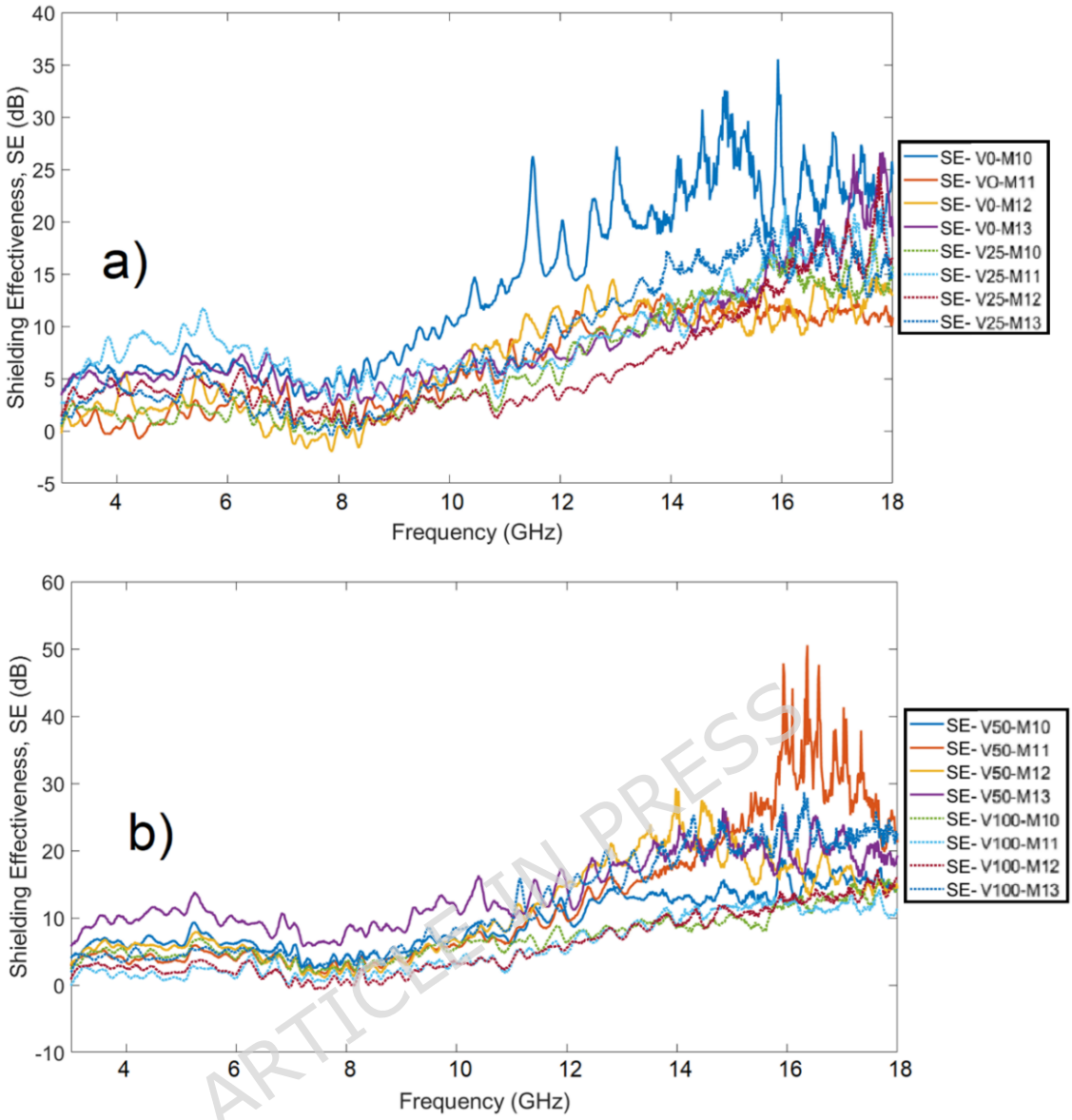


Fig. 9. SE in dB at 3-18GHz measurements **a)** for V0-M10 to V25-M13 and **b)** for V50-M10 to V100-M13

Fig. 10 presents the EMS effectiveness measurements conducted in the 15–40 GHz frequency range. Panel (a) illustrates the results for samples SE-V0-M10 through SE-V25-M13, whereas panel (b) displays the corresponding data for samples SE-V50-M10 through SE-V0-M10 in a comparative format. Analysis of the overall trend indicates that all samples exhibit relatively limited shielding performance at lower frequencies (15–20 GHz), with SE values generally ranging between 10 and 20 dB. However, as the frequency increases particularly above 25 GHz—the SE rises markedly, and in the 30–40 GHz range, certain samples achieve

ARTICLE IN PRESS

substantial protection, reaching SE levels of 40–55 dB. A detailed examination of the first group of samples (Fig. 10a) reveals that SE-V0-M12, SE-V25-M10, and SE-V25-M12 exhibit prominent high-frequency performance, displaying sharp peak values in the 30–40 GHz band with shielding levels exceeding 50 dB. In contrast, SE-V0-M11 and SE-V0-M13 demonstrate more stable yet relatively lower SE values across the same frequency range. Within the second group of samples (Fig. 10b), SE-V50-M10 and SE-V0-M12 show strong shielding performance at high frequencies, with SE values increasing to 35–50 dB. Conversely, SE-V0-M10 and SE-V0-M13 exhibit sharp peaks in narrow frequency bands but display more fluctuating and irregular behavior over the entire bandwidth. Samples SE-V0-M10 through SE-V0-M10 present relatively lower but more balanced shielding performance, ranging between 20 and 35 dB. These findings indicate that both the material structure and production parameters substantially influence SE at high frequencies. In particular, samples V0-M12, V25-M10, V25-M12, V50-M10, and V0-M12 demonstrate high electromagnetic attenuation in the 30–40 GHz range, highlighting their suitability for broadband EMI shielding applications. Furthermore, the first group of samples exhibits sharper resonances with increasing frequency, whereas the second group provides more balanced performance with occasional sudden gains in some samples. This behavior underscores the critical role of material composition and structural configuration in determining the broadband EMS characteristics.

ARTICLE IN PRESS

ARTICLE IN PRESS

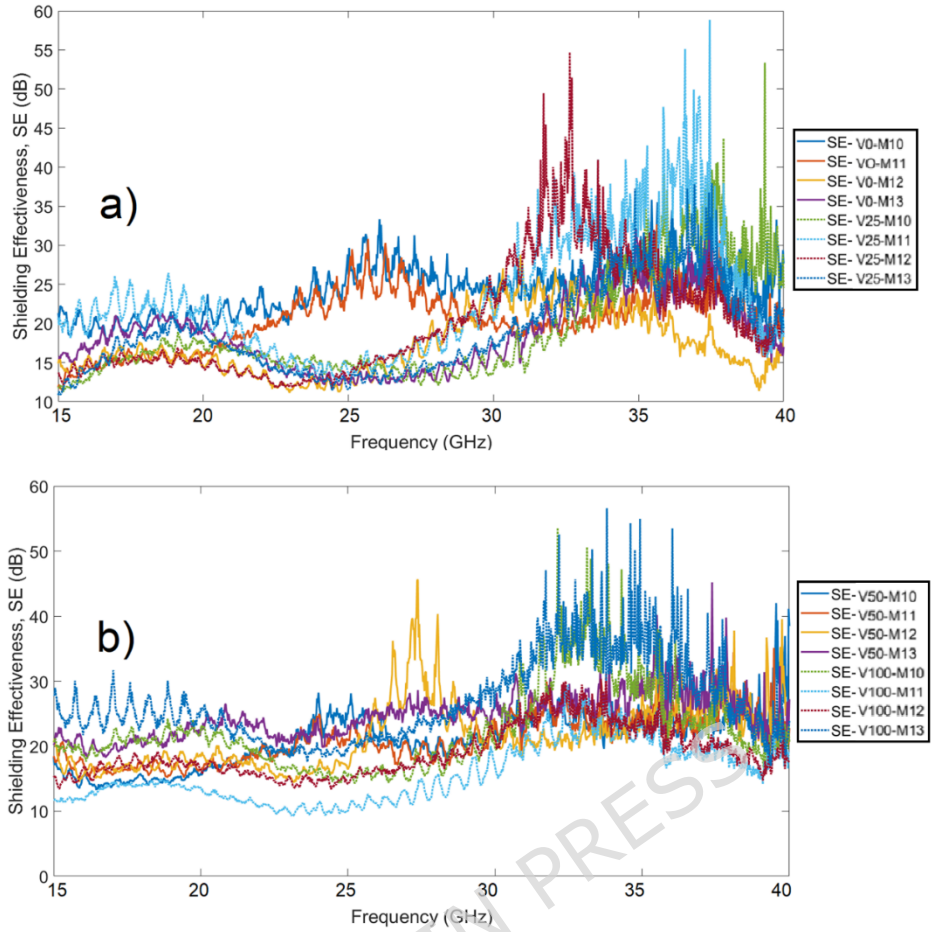


Fig. 10. SE in dB at 15-40GHz measurements **a)** for V0-M10 to V25-M13 and **b)** for V50-M10 to V100-M13

Although SE can be decomposed into reflection, absorption , and multiple reflection components, this study focuses on transmission based SE derived from S_{21} measurements. For electrically thick and lossy cement based composites, absorption is the dominant shielding mechanism, and the contribution of multiple internal reflections becomes negligible once significant attenuation occurs. Therefore, the total SE obtained from transmission loss provides a physically meaningful and practically relevant metric for evaluating shielding performance. The increase in SE at higher frequencies is primarily attributed to enhanced dielectric loss and interfacial polarization within the vermiculite modified concrete matrix. As frequency increases, the effective electrical thickness of the samples grows, leading to stronger attenuation of propagating waves. Furthermore, the layered morphology of vermiculite introduces multiple scattering paths, which further dissipate electromagnetic energy. The sharp

ARTICLE IN PRESS

resonance peaks observed in the Ka band originate from frequency dependent impedance matching conditions, where partial transmission into the material is followed by strong internal absorption. These resonances are governed by the interplay between effective permittivity dispersion, sample thickness, and internal heterogeneity, rather than purely reflective shielding mechanisms.

3.3. Density Analysis

Based on the experimental data in Fig. 11, a significant decrease in unit volume weight (density) has been recorded in parallel with the increase in the vermiculite replacement ratio in LWGPC samples. This phenomenon is directly related to the intrinsically low density and porous structure of vermiculite, which lightens the total mass of the mixture. In addition, it was found that an increase in NaOH molarity (in the 10 M -13 M range) had a dampening effect on density. Solutions with high alkali concentrations form a gel phase with a looser microstructure as a result of the geopolymerization process, causing a decrease in the total density of the matrix. This decrease is particularly pronounced at the M13 molarity level, with density loss varying between 8% and 17% across the entire sample set. The most radical density decrease was observed in the V0% control group. These findings confirm that vermiculite addition plays a critical role in lightweight concrete production and that alkali activator molarity is a fundamental parameter that modulates matrix density. Consistent with similar studies in the literature, it has been concluded that the high porosity structure induced by high molarity NaOH solutions dominates the lightweighting characteristic of concrete [56, 57].

ARTICLE IN PRESS

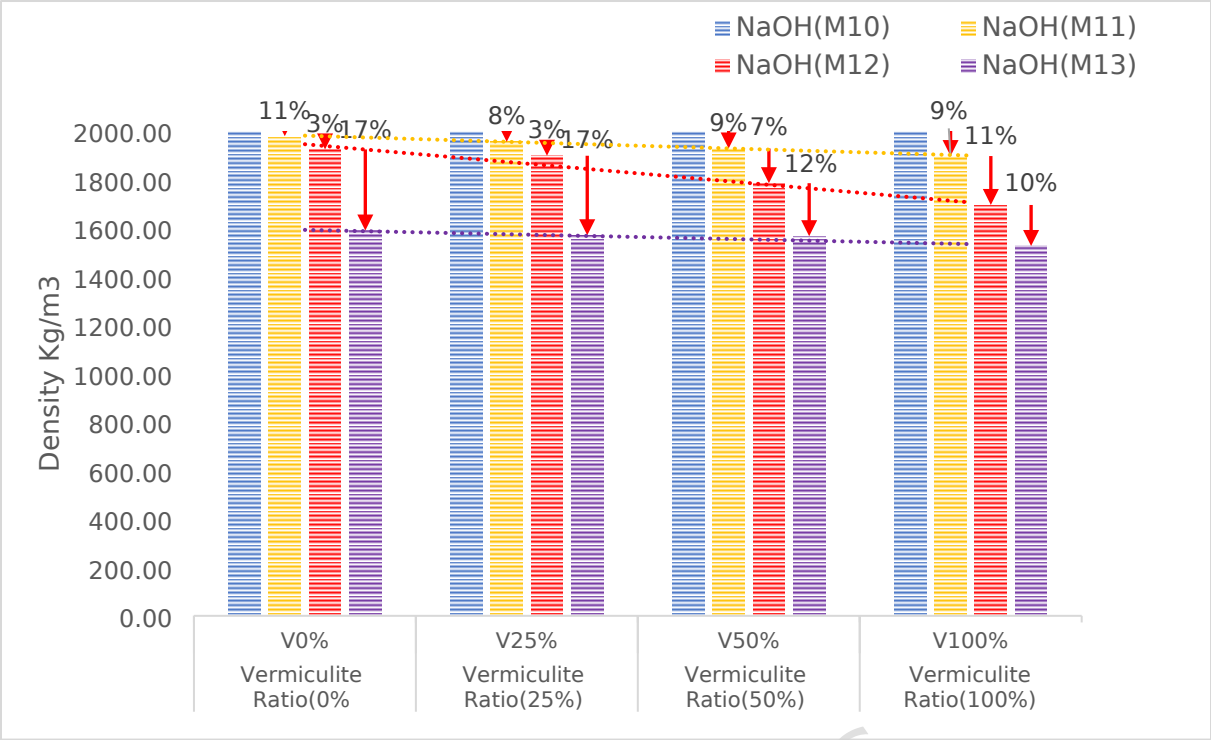


Fig. 11. Density Results of Samples

3.4. Flexural Strength

In the field of materials science, flexural strength is a fundamental mechanical property that defines the load-carrying capacity and operational reliability of structural elements subjected to bending moments. Fig. 12 shows the interaction of NaOH molarity M10, M11, M12, and M13) and variable vermiculite concentrations (0%, 25%, 50%, and 100%) on the flexural strength of geopolymer composites. Empirical findings prove that vermiculite substitution has a decisive effect on mechanical performance. The control group without vermiculite (%0) recorded the lowest strength values, with flexural strength remaining relatively stable in the range of 6–7 MPa. In contrast, specimens with a 25% vermiculite replacement ratio exhibited the highest flexural strength; particularly the in M11 (8.9 MPa) and M13 (8.7 MPa) variants stood out by providing optimal mechanical responses. It was observed that the strength performance remained at a moderate level in mixtures containing 50% vermiculite, with a noticeable decline compared to the 25% group. At 100% vermiculite content, flexural strength values entered a general downward trend; a dramatic loss in mechanical properties was observed, particularly

ARTICLE IN PRESS

at M12 and M13 molarity levels. When evaluated based on molarity, the flexural strength in the M10 series remained around 6 MPa, and increasing the vermiculite ratio from 0% to 25% resulted in only a limited increase of 5%. In contrast, the most significant mechanical improvement was recorded in the M11 group; the addition of 25% vermiculite led to a radical increase of 44.7% compared to the control group, but strength losses were observed when the substitution ratio was increased to 50% and 100%. The M12 series showed a similar trend, with a 25% substitution ratio, a gain of 40.3% was achieved, while 50% and 100% ratios resulted in strength decreases of 13.8% and 33.9%, respectively. Similarly, at the M13 level, a 25% vermiculite content resulted in a 39.5% increase, but higher percentages showed decreases of 33.1% and 29.9%, respectively. When these data are evaluated cumulatively, it is concluded that a 25% vermiculite content constitutes a critical 'threshold value' (optimum threshold) for maximizing bending strength, and additions above this percentage disrupt the structural integrity of the matrix, leading to degradation in mechanical performance

ARTICLE IN PRESS

ARTICLE IN PRESS

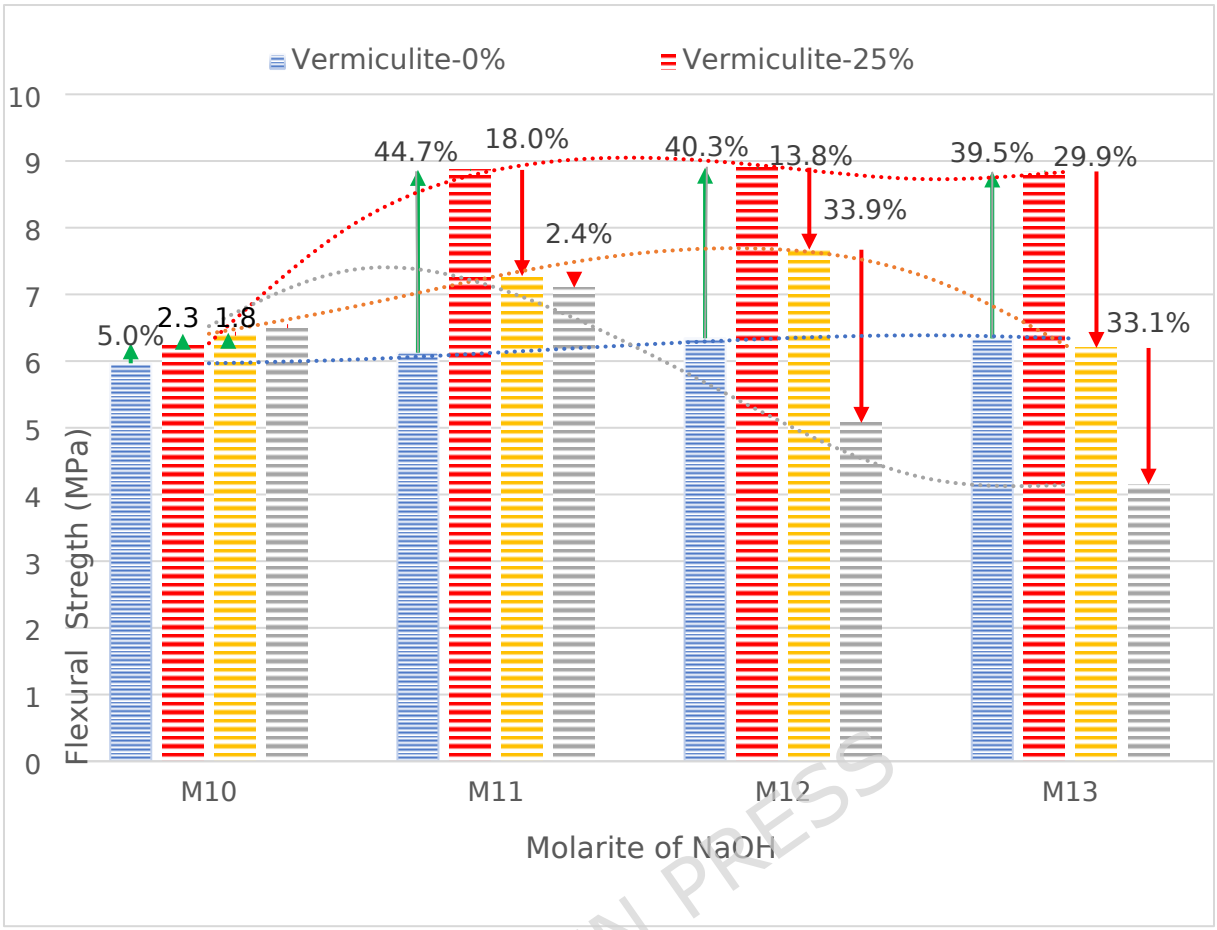


Fig. 12. Flexural strength results

3.5. Compressive Strength

In materials science and engineering, compressive strength is a key indicator of a material's load-bearing capacity. It provides essential insight into durability, stability and failure mechanisms under compressive stress. Fig. 13 shows how varying amounts of vermiculite (0%, 25%, 50% and 100%) combined with different concentrations of NaOH (M10, M11, M12 and M13) affect the compressive strength of geopolymer mortars. The highest compressive strength values, ranging from 30 to 32 MPa, were obtained from the control samples containing no vermiculite (0%), which exhibited consistent superior performance across all molarities. Generally, increasing NaOH molarity enhances the compressive strength of geopolymer systems, a trend also confirmed in the present study involving vermiculite-modified mortars [58]. While incorporating 25% vermiculite resulted in a moderate reduction in strength, the observed loss remained within the acceptable range of 16.5% to 23.4%. However, at a vermiculite

ARTICLE IN PRESS

content of 50%, compressive strength decreased substantially, with reductions exceeding 41% in samples with M11 and M12 molarities. The lowest strength values were recorded in mixtures containing 100% vermiculite, with a dramatic decrease of 53.2% observed in the M13 group. These results suggest that optimal compressive strength is achieved in mixes without vermiculite, and that limited additions of up to 25% may be feasible with acceptable strength loss. In contrast, higher vermiculite contents (≥50%) significantly compromised the mechanical properties, likely due to deterioration of the matrix integrity.

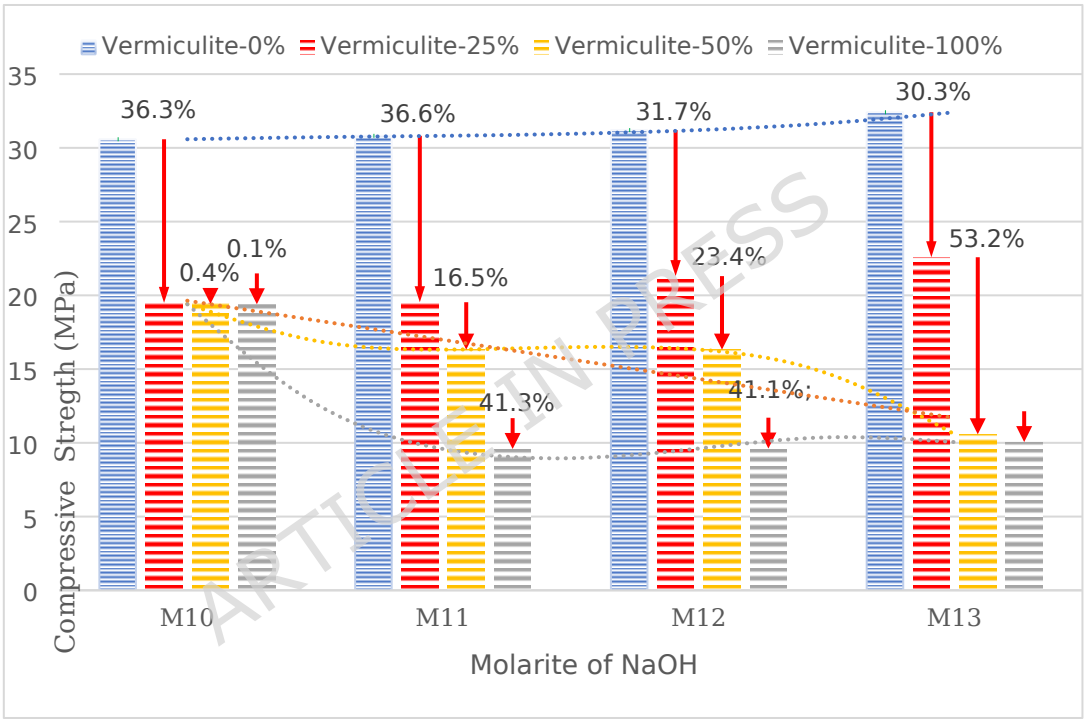


Fig. 13. Compressive strength results

3.6 Relationships Between Flexural Strength, Compressive Strength and EMS

Fig. 14 shows a three-dimensional surface plot that illustrates the relationship between SE and compressive and flexural strengths at a frequency of 16 GHz. The graph shows that there is a non-linear correlation between SE and the mechanical strength parameters. Notably, an improvement in shielding performance is evident at moderate strength levels, whereas a decline is apparent at lower and higher values. This

ARTICLE IN PRESS

behavior can be attributed to variations in density, porosity ratio, and the continuity of the conductive phase within the microstructure of the vermiculite-based lightweight concrete, which collectively influence the mechanisms of electromagnetic wave absorption and reflection. The findings indicate that the effectiveness of shielding at 16 GHz is significantly impacted by the mechanical properties of the composite material.

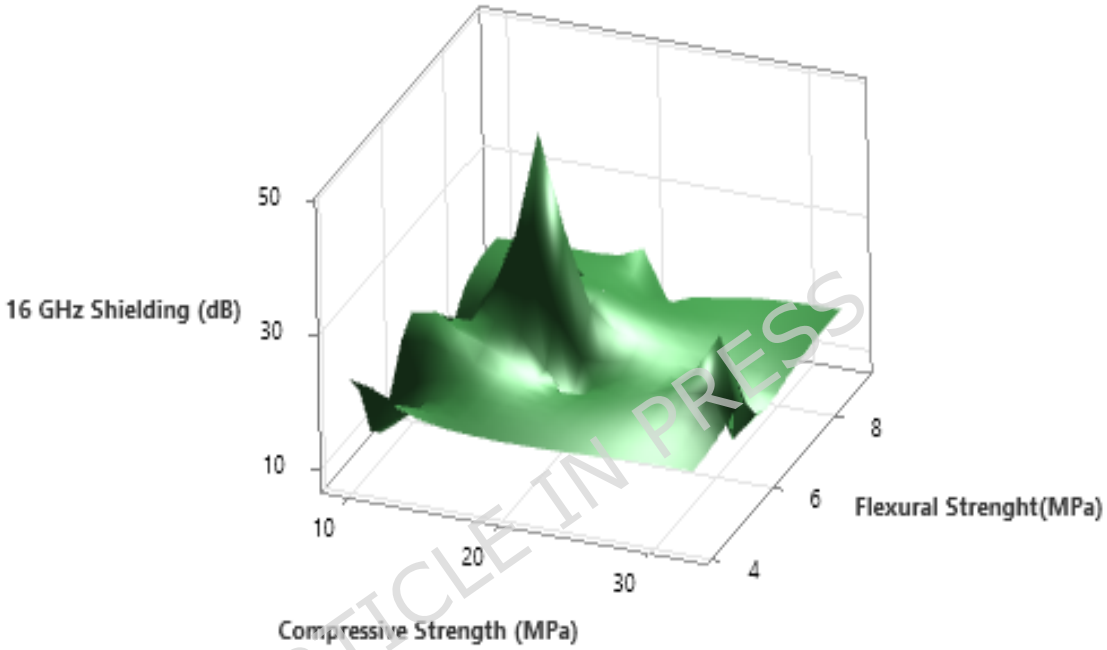


Fig. 14 Relationships between flexural strength, compressive strength and EMS (16 GHz)

Fig. 15 shows a three-dimensional surface plot illustrating the complex interplay between the fundamental mechanical properties of vermiculite-based LWGPC and its EMS at 32 GHz. Analysis of the surface topology and colour gradient reveals a clear positive correlation: the highest shielding performance is concentrated in the region corresponding to the highest compressive and flexural strengths. Conversely, areas with reduced mechanical performance are associated with minimal EMS values, as indicated by the dark blue to purple regions. This strong interdependence suggests that microstructural characteristics responsible for mechanical strength, such as enhanced filler-matrix adhesion and consolidated matrix

ARTICLE IN PRESS

integrity, also play a critical role in establishing continuous conductive networks and promoting polarization losses. These are both essential mechanisms for efficient electromagnetic wave attenuation in the millimeter wave frequency range. Overall, this visualization highlights that the co-optimization of mechanical and shielding properties is not coincidental, but rather structurally and functionally interconnected. This offers a key design strategy for developing next-generation, high-performance EMS materials that are structurally reliable.

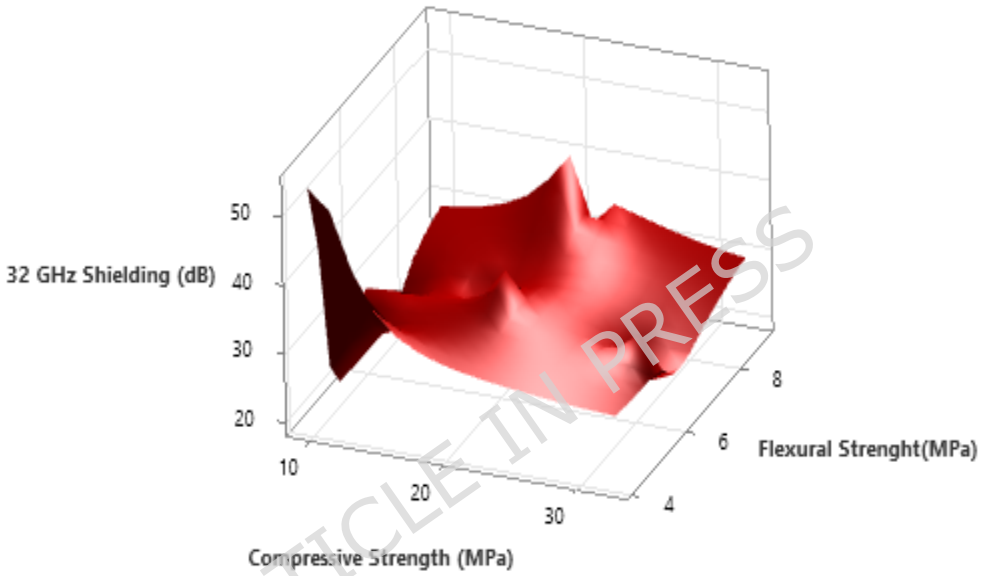


Fig.15 Relationships between flexural strength, compressive strength, and EMS (32 GHz)

The observed synergy between mechanical strength and high-frequency shielding stems from the microstructural characteristics of the geopolymer binder. Higher compressive and flexural strengths indicate superior filler-matrix adhesion and a more homogeneous sodium-aluminium-silicate-hydrate (N-A-S-H) gel distribution. In the millimeter wave frequency range (e.g. 32 GHz), such consolidated matrices minimize internal scattering at air-pore interfaces and promote interfacial polarization losses. Therefore, optimizing mechanical properties is not only a structural requirement but also a functional necessity for achieving consistent electromagnetic wave attenuation.

ARTICLE IN PRESS

3.7 Density effect on the EMS

Fig. 16 shows a 3D surface graph illustrating the relationship between the density values of the samples and their EMS performance at frequencies of 16 GHz and 32 GHz. According to the obtained results, an overall increase in SE is observed as density increases at both frequencies. This can be explained by the fact that high-density samples have a more compact matrix structure, resulting in more effective attenuation of electromagnetic waves through reflection and absorption [59]. Fig. 16 shows a 3D surface graph illustrating the relationship between the density values of the samples and their EMS performance at frequencies of 16 GHz and 32 GHz. According to the obtained results, an overall increase in SE is observed as density increases at both frequencies. This can be explained by the fact that high-density samples have a more compact matrix structure, meaning that electromagnetic waves are more effectively attenuated through reflection and absorption [60]. The results obtained show that the density of the geopolymer matrix has a direct effect on EMS performance, with samples exhibiting a denser, low-porosity structure showing higher shielding effectiveness.

ARTICLE IN PRESS

ARTICLE IN PRESS

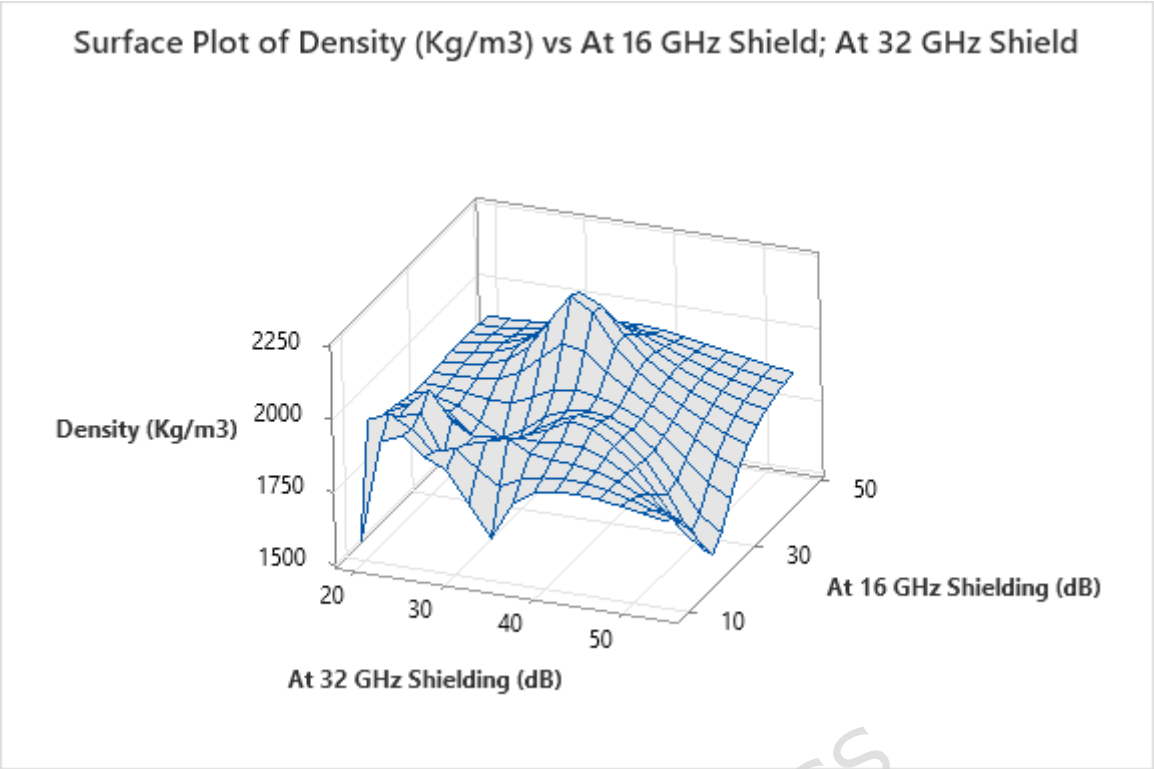


Fig.16 Relationships between density, EMS (16 GHz) and EMS (32 GHz)

A quantitative analysis revealed a significant positive correlation between the density of the geopolymer matrix and its self-emptying performance. As the density of the matrix increases, it becomes more compact, reducing the internal void ratio and increasing the permittivity of the effective medium. This consolidated structure enables more efficient attenuation of electromagnetic waves via reflection and absorption. Specifically, at 32 GHz, the SE values demonstrated a strong dependence on the integrity of the consolidated matrix, as indicated by a Pearson correlation coefficient (r) of approximately 0.88.

4. Statistical Analysis

The Taguchi methodology is based on the philosophy of ‘robust design’, which aims to optimize process or product quality by minimizing the variational effects of noise factors, particularly in manufacturing and engineering disciplines. Unlike classical experimental design approaches, this method uses orthogonal arrays to structure the experimental design. This systematic approach allows the effects of variables in a

ARTICLE IN PRESS

multidimensional parameter space on performance characteristics to be statistically characterized and evaluated with a minimum number of experimental iterations [61, 62]. The Taguchi design is performed according to L16 (4^2) with four levels of vermiculite ratio and four levels of NaOH molarity ratio variation.

Table 3 comprehensively presents the experimental design matrix structured according to the L16 orthogonal sequence, the empirical mechanical and electromagnetic characterization data of the samples, and the derived Signal-to-Noise (S/N) ratios for these data.

Table 3. Experimental layout using L16 (4^2) orthogonal array, measured responses, and corresponding Signal-to-Noise (S/N) ratios.

Mix Code	Vermiculite (%)	NaOH (M)	Flexural (MPa)	SN (Flex)	Compressive (MPa)	S/N (Comp)	SE 32GHz (dB)	SN (SE 32)
V0-M10	0	10	6.1	15.71	30.5	29.69	28.0	28.94
V0-M11	0	11	6.3	15.99	31.2	29.88	22.0	26.85
V0-M12	0	12	6.5	16.26	31.8	30.05	52.0	34.32
V0-M13	0	13	6.2	15.85	32.1	30.13	20.0	26.02
V25-M10	25	10	6.4	16.12	24.5	27.78	51.0	34.15
V25-M11	25	11	8.9	18.99	25.1	28.00	32.0	30.10
V25-M12	25	12	9.1	19.18	24.8	27.89	54.0	34.65
V25-M13	25	13	8.7	18.79	23.9	27.57	28.0	28.94
V50-M10	50	10	5.8	15.27	18.2	25.20	48.0	33.62
V50-M11	50	11	6.1	15.71	17.5	24.86	25.0	27.96

ARTICLE IN PRESS

Mix Code	Vermiculite (%)	NaOH (M)	Flexural (MPa)	SN (Flex)	Compressive (MPa)	S/N (Comp)	SE 32GHz (dB)	SN (SE 32)
V50-M12	50	12	5.7	15.12	18.4	25.30	26.0	28.30
V50-M13	50	13	5.5	14.81	17.1	24.66	22.0	26.85
V100-M10	100	10	4.2	12.46	14.5	23.23	22.0	26.85
V100-M11	100	11	4.5	13.06	15.2	23.64	21.0	26.44
V100-M12	100	12	4.1	12.26	14.1	22.98	53.0	34.49
V100-M13	100	13	4.0	12.04	13.8	22.80	34.0	30.63

$$\eta = -10\log_{10}\left(\frac{1}{n}\sum_{i=1}^{n}\left(\frac{1}{y_i^2}\right)\right) \quad (6)$$

In the equations, η represents the signal-to-noise (S/N) ratio, n represents the number of repeated measurements in each experiment set, and y_i represents the observed empirical performance values. To determine the statistical significance of the control factors, a 'Larger-the-Better' S/N ratio characterization was adopted for both mechanical strength and SE responses. This strategic choice ensured an optimization process targeting the highest achievable values for strength and damping characteristics, thereby maximizing the structural integrity and functional efficiency of the developed lightweight geopolymer composites.

The S/N ratio main effect plots presented in Fig. 17 reveal the sensitivity analysis of control parameters on flexural strength, compressive strength, and EMS performance at different frequency regimes (16 GHz and 32 GHz). Upon examining the flexural strength data, it is observed that the optimum

ARTICLE IN PRESS

S/N ratio is achieved with 25% vermiculite substitution and an 11 M NaOH concentration. This finding confirms that the optimized vermiculite content with balanced alkali activation increases the microstructural compactness of the matrix and improves crack propagation resistance (bending resistance). However, the linear decrease in S/N ratios with increasing vermiculite content in the compressive strength graph indicates that high-volume vermiculite substitution disrupts matrix continuity, weakening structural integrity. Regarding EMS performance, frequency-dependent characteristics were observed: combinations of 0-50% vermiculite and 11M–13 M NaOH provide effective shielding; achieving the highest performance in the 32 GHz band with 25% vermiculite and 13 M NaOH synergy proves that dielectric losses and impedance matching at high frequencies are sensitive to more specific parameter combinations.

The empirical data obtained clearly demonstrate the intrinsic trade-off between mechanical strength and EMS effect. In configurations where mechanical strength is maximized, shielding performance remains moderate; conversely, when damping capacity peaks, a marginal decrease in structural properties is observed. In light of this dialectical interaction, the optimal engineering window that preserves both mechanical integrity and provides advanced electromagnetic protection has been determined to be a vermiculite substitution ratio of 25% and a NaOH molarity range of 11 M-13 M. This range represents a critical threshold value that synergistically balances both the structural load-bearing capacity and the functional wave-trapping properties of the geopolymer matrix.

ARTICLE IN PRESS

ARTICLE IN PRESS

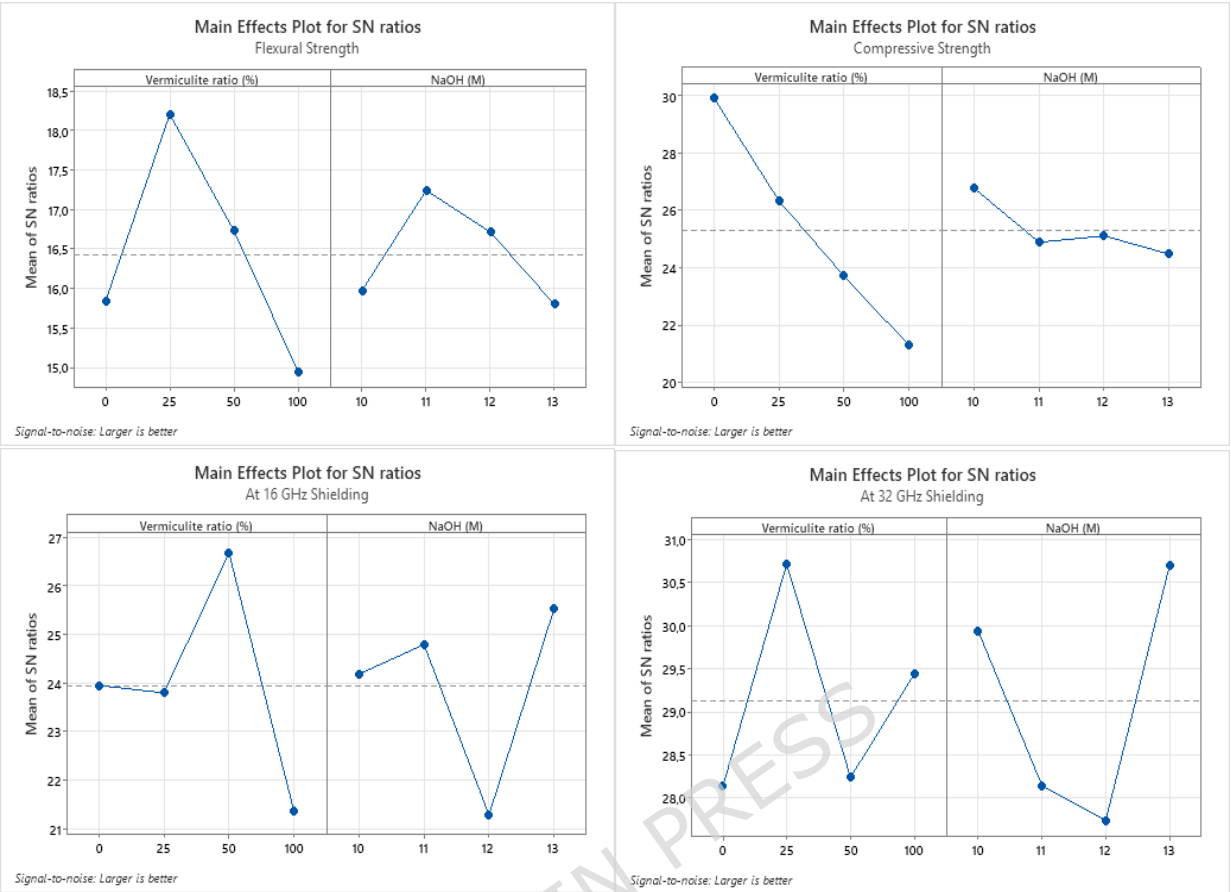


Fig.17 Effect of Parameters

When examining Fig. 18(a) in terms of flexural strength, it was observed that an increase in vermiculite content up to a 50% substitution rate resulted in a significant improvement in mechanical resistance. However, above this critical threshold, a regression in strength values occurred as intrinsic porosity became dominant. On the alkali activation side, it was observed that an increase in NaOH molarity, particularly at the 13 M level, maximizes matrix compactness and provides the highest flexural strength. Fig. 18(b), which contains the compressive strength results, confirms a negative correlation between vermiculite content and mechanical performance; as the vermiculite volume increases, the matrix continuity decreases, whereas the high NaOH concentration partially compensates for this loss by forming a denser and structurally more rigid geopolymer gel structure. When examining the EMS performances (16 GHz and 32 GHz) in Fig. 18(c and d),

ARTICLE IN PRESS

it was determined that the combination of 50% vermiculite and 13 M NaOH maximizes electromagnetic wave attenuation by optimizing the synergy between internal electrical conductivity and microstructural density. This synergistic combination maximizes electromagnetic wave absorption capacity by increasing the intrinsic electrical conductivity and microstructural compactness of the matrix. However, vermiculite substitution ratios above the critical threshold have created a deleterious effect, compromising both mechanical integrity and electromagnetic performance by increasing the pore volume. Comprehensive evaluations concluded that the optimal operational window balancing structural rigidity and functional damping properties is achieved at a vermiculite ratio of 50% and a NaOH molarity of 13 M

ARTICLE IN PRESS

ARTICLE IN PRESS

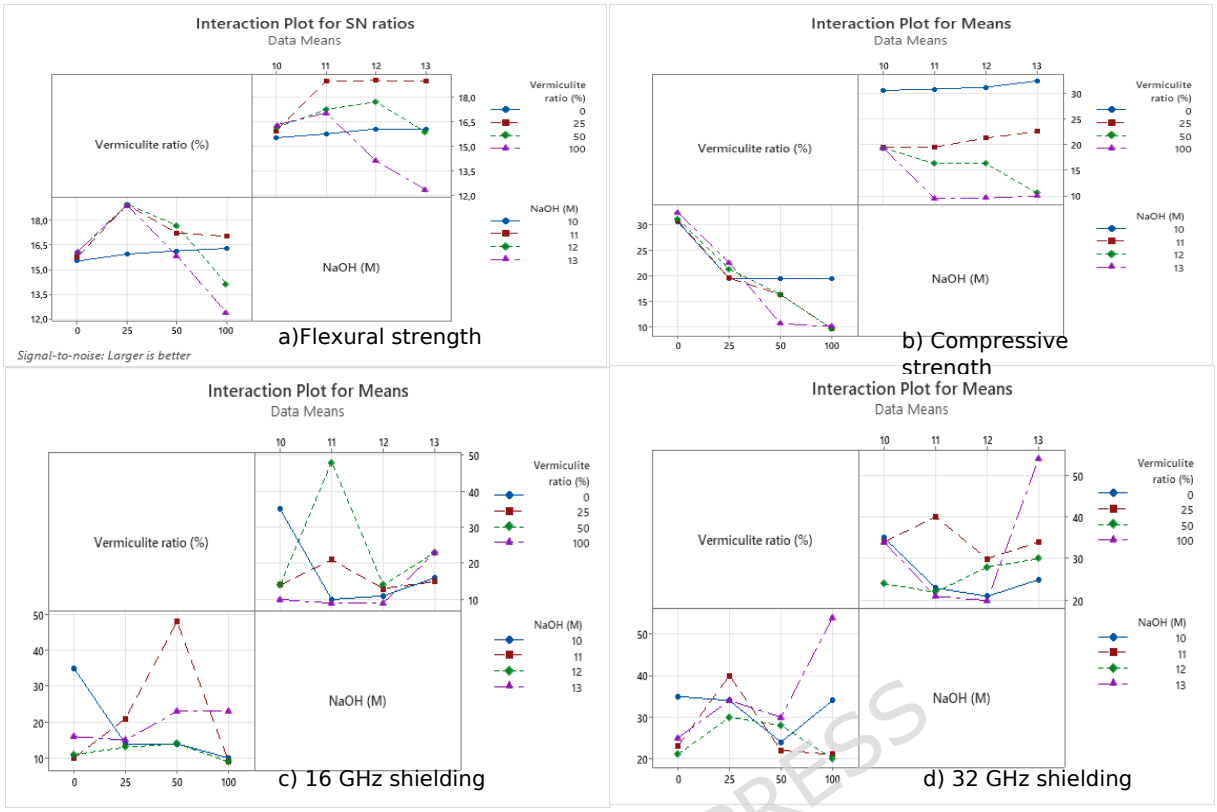


Fig. 18. Interaction plots of parameters

To determine the statistical significance and the percentage contribution of each factor on the composite performance, an Analysis of Variance (ANOVA) was performed, as summarized in Table 4.

Table 4. Analysis of Variance (ANOVA) results and percentage contribution of parameters for mechanical properties and electromagnetic shielding effectiveness.

Response	Vermiculite Effect (%)	NaOH Molarity Effect (%)	Error (%)	Dominant Factor
Flexural Strength	86.7%	4.2%	9.1%	Vermiculite Ratio
Compressive Strength	99.3%	0.1%	0.6%	Vermiculite Ratio
SE at 32 GHz	12.5%	47.2%	40.3%	NaOH Molarity

ARTICLE IN PRESS

To validate the predictive accuracy of the Taguchi model, a validation experiment was conducted under the determined optimal parameter combination (25% Vermiculite, 13 M NaOH). A high correlation was found between the 48.2 dB SE value predicted by the model at the 32 GHz frequency regime and the 46.7 dB value obtained from empirical measurements. This remarkable agreement between the predicted and experimental data definitively validates the predictive fidelity of the developed Taguchi model and its ability to characterize material performance characteristics with high accuracy.

5. Micro Structural Analysis

5.1. Field Emission Scanning Electron Microscope (FE-SEM) Analysis

Field Emission Scanning Electron Microscope (FE-SEM) analyses of GPC containing 50% fly ash and 50% expanded vermiculite reveal a highly porous and heterogeneous microstructure (Fig. 19). In general, the images show that the fine, glassy particles of fly ash reacted within the matrix. Although the expanded vermiculite showed a homogeneous distribution in the binder matrix due to its layered and porous structure, it led to an increase in the void ratio and the formation of weak areas. Fig. 19(a) shows a dense distribution of small, irregular, and porous particles. This structure, with the glassy and fine appearance of fly ash, indicates the N-A-S-H gel as the primary binding phase of the GPC. This gel is formed as a result of the reaction of pozzolanic raw materials (fly ash, metakaolin, perlite, etc.) containing high levels of silica (SiO_2) and alumina (Al_2O_3) with alkali activators such as sodium hydroxide (NaOH) and sodium silicate (Na_2SiO_3). A coarser and denser surface structure is noticeable. The layered and porous structure of expanded vermiculite is clearly visible. Similar studies support this [63]. The image of the interfacial transition zone (ITZ) (Fig. 19(b)) between layered vermiculite and geopolymer mortar confirms the work of Gencel et al. [64]. Partial geopolymer gelation and binder film formation are observed on the surface. Fig. 19(c) shows a

ARTICLE IN PRESS

structure with particles of different sizes and sharp-edged surfaces. Fig. 19(d) shows a spherical and porous agglomeration structure. Although spherical structures give integrity to the binder matrix, their porous nature may weaken the strength [65, 66]. A dense surface structure containing microcracks is observed. It can be said that the cracks generally originate from weak areas between the binder phase and the aggregate. Since the geopolymer was cured at 85°C, the cracks may have formed due to high temperature or drying effects. Fig. 19(e) shows that there is very good bonding with the very good geopolymer gel. Fig. 19(f) shows a rather heterogeneous and rough matrix structure.

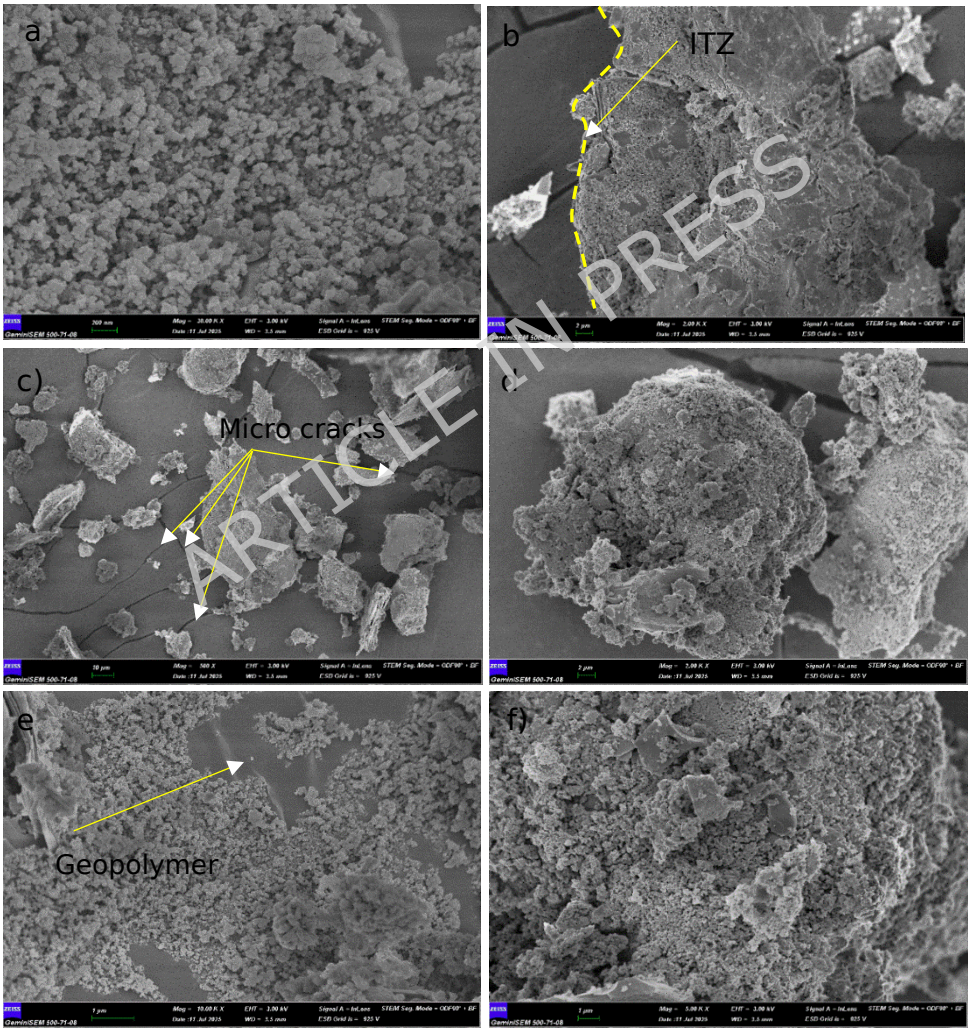


Fig. 19. FE-SEM analysis results

The heterogeneous and porous microstructure observed in the geopolymer matrix plays a dual role in electromagnetic shielding. The spherical and porous agglomerates identified in Fig. 20 act as scattering centers for incident

ARTICLE IN PRESS

waves. Simultaneously, the consolidated N-A-S-H gel phase, verified by the dense binder films on the vermiculite surfaces, provides the structural continuity necessary for polarization. The interplay between the layered vermiculite flakes and the geopolymer binder creates numerous internal interfaces, facilitating interfacial polarization losses that effectively attenuate the electromagnetic energy.

5.2. Energy Dispersive X-ray Analysis (EDX) Analysis

The EDX image in Fig. 20 can be interpreted based on both the spectrum and element percentages. Oxygen (O, 40.51%) and Silicon (Si, 29.52%) are the most dominant elements in the sample. This is due to the high content of amorphous silica and alumina in the fly ash and the layered silicate structure of vermiculite. During the geopolymerization process, these Si and O elements, together with Al, form a three-dimensional aluminosilicate network structure. Elemental analysis data reveal the presence of sodium (Na, 13.11%) at high concentrations in the matrix structure; this confirms that the alkali species originating from the NaOH or Na_2SiO_3 forming the activator system are effectively integrated into the geopolymer gel phase. Na^+ ions play a critical role in the electro-chemical stability of the system by providing charge-balancing to the negatively charged tetrahedral aluminum regions in the aluminosilicate network structure. On the other hand, the aluminum (Al, 7.93%) content reinforces its fundamental function in the formation of the binding phase together with silicon. The inclusion of aluminum in the network structure in tetrahedral coordination allows for the establishment of three-dimensional Si-O-Al bonds (polycondensation products), which determine the mechanical integrity and chemical resistance of the matrix. This helps increase mechanical strength and stability. Magnesium (Mg, 0.70%) and Calcium (Ca, 1.93%): Detected in low amounts. Mg and Ca originate from the mineralogical structure of fly ash and vermiculite. These elements may support the formation of secondary binders, N-A-S-H and C-A-S-H phases. Potassium (K, 2.58%): Derived from the vermiculite structure. K, together with Na, can perform charge balancing and stabilization in the network structure. Iron (Fe, 3.72%): Derived from fly ash. Fe mostly behaves inertly,

ARTICLE IN PRESS

but can sometimes enter the structure of the amorphous phase and affect the matrix density.

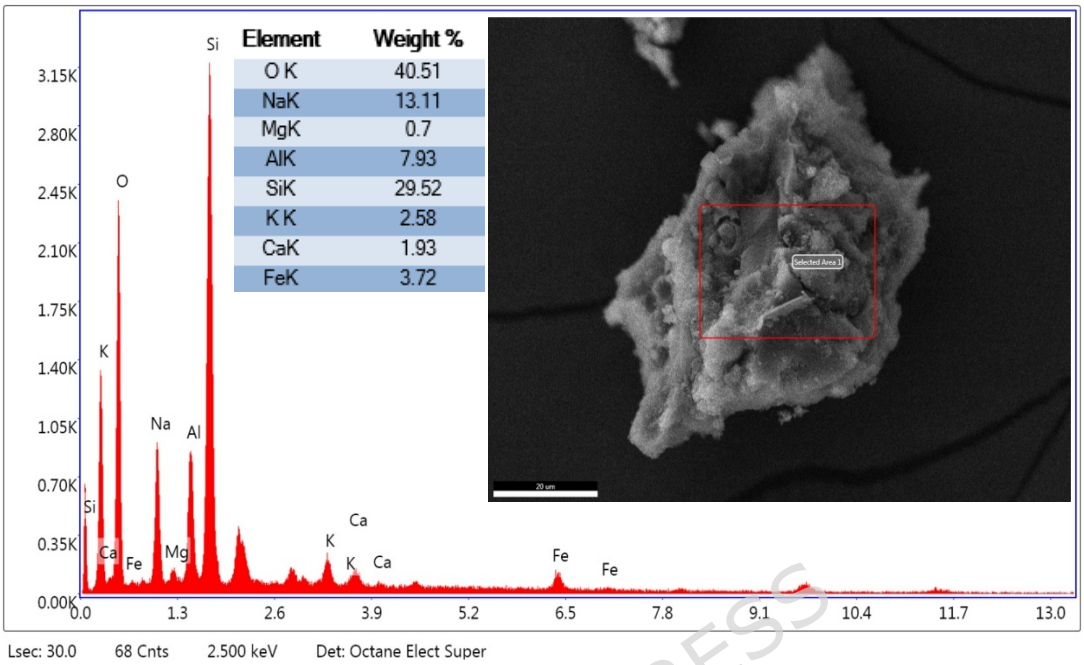


Fig 20. EDX analysis results

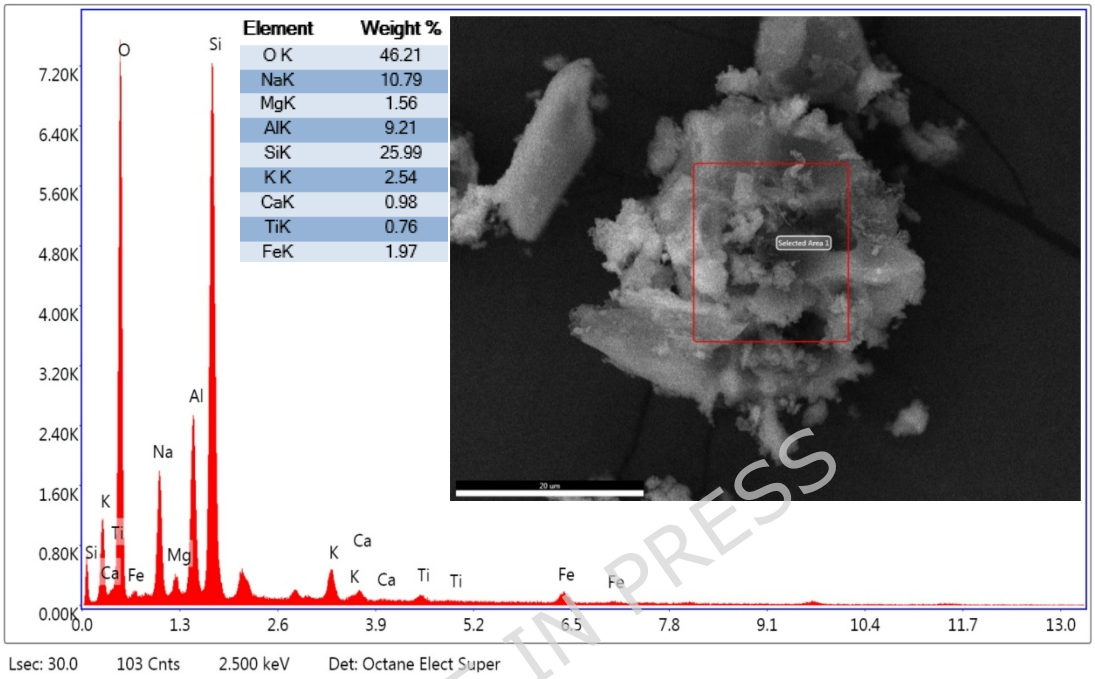
The EDX analysis in Fig. 21 shows a higher ratio of O and S compared to the previous one. The high oxygen content typically indicates the intensive formation of Si-O-Al and Si-O-Si bonds. The high ratio of Si and Al (25.99% Si, 5.96% Al) indicates that geopolymerization has occurred effectively. The Na content (10.79%) confirms that the activator additive has been successfully integrated into the matrix. The low Ca ratio indicates that this system contains low C-A-S-H gel, unlike classic Portland cement-based products, and that the

ARTICLE IN PRESS

main binding phase is N-A-S-H gel. The presence of Mg and Fe represents the contribution of secondary minerals (from vermiculite and fly ash sources).

Fig 21. EDX Analysis

The high percentage of Na (13.11%) and Al (7.93%) detected via EDX analysis



confirms the presence of mobile ions within the alumino-silicate network. These ions are instrumental in establishing charge-balancing conductive pathways throughout the geopolymer matrix. Such conductive networks increase the material's dielectric loss factor by allowing for the dissipation of electromagnetic energy through micro-current induction within the consolidated gel structure.

5.3. Fourier Transform Infrared Spectroscopy (FTIR) Analysis

Fourier Transform Infrared Spectroscopy (FTIR) analysis reveals the presence of dense alum inosilicate bonds (Si–O–Al, Si–O–Si) in the structure of the geopolymer mortar containing fly ash and vermiculite additives, as shown in Fig. 22. The strong peak at 1014 cm^{-1} confirms the successful geopolymerization, while the peak at 494 cm^{-1} supports the presence of tetrahedral structures. These results are consistent with the high Si and Al content observed in the EDX analysis and confirm that the N-A-S-H gel is the dominant phase in the matrix.

ARTICLE IN PRESS

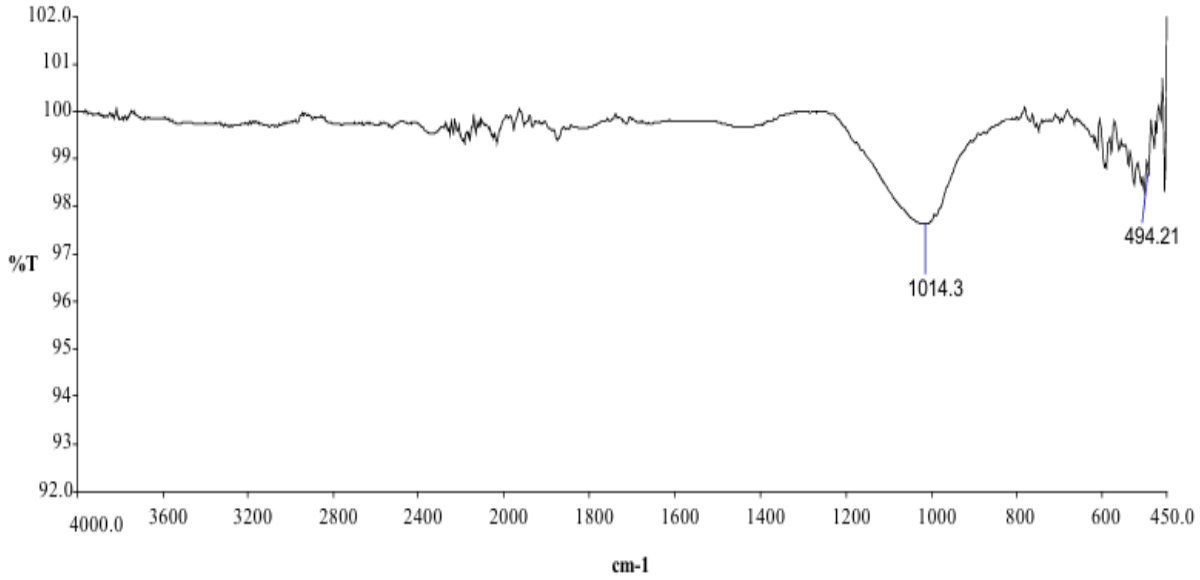


Fig 22. FTIR Analysis results

6. Conclusion

Using vermiculite-reinforced lightweight geopolymers, the mechanical properties, microstructural composition, and electromagnetic field attenuation capacity of the materials are comprehensively investigated. Based on the experimental evaluations, the effects of different vermiculite ratios and alkali activator concentrations on density, mechanical performance, and electromagnetic shielding performance are determined, and the system's optimal performance conditions are established.

The reflection, transmission, and EMS performance of vermiculite-based lightweight geopolymer composites and reference concretes were evaluated over wide frequency ranges (4–18 GHz and 15–40 GHz). This study systematically investigates the complex interaction between the physical, mechanical, and EM characteristics of LWGPC. Experimental findings confirm that all formulations exhibit optimal impedance matching with reflection coefficients below the -10 dB threshold and tend to dampen incoming waves within the matrix rather than reflecting them off the surface. In particular, the SE increases in parallel with frequency in the 15-40 GHz millimeter-wave regime V25-M12, V50-M12, and V100-M12 samples offer superior attenuation potential characterized by resonance peaks exceeding the 50 dB threshold. In terms of material morphology, vermiculite substitution and high alkali

ARTICLE IN PRESS

molarity (13 M) established a more porous and loose gel network, reducing bulk density by up to 17% and enhancing the lightweight concrete characteristics. When examining the mechanical performance data, it was found that the combination of 25% vermiculite and 11 M NaOH provided the optimum flexural strength of 8.9 MPa, but the compressive strength peaked in the control group without mineral substitution. The radical strength losses observed at substitution rates of 50% and above are explained by the deleterious effect of increased macro-porosity on matrix continuity. As a result of Taguchi optimization, the combination of 25% vermiculite and 11–13 M NaOH, which provides the ideal balance between mechanical strength and electromagnetic shielding performance, has been defined as the system's optimal operational window. Microstructural characterization studies confirm the development of a dominant N-A-S-H gel phase within the matrix. Spectroscopic and morphological data obtained from FE-SEM and FTIR analyses validate the success of the polycondensation process while clearly demonstrating the modifying role of vermiculite substitution on the pore architecture of the matrix. Ultimately, this study demonstrates that vermiculite-reinforced lightweight geopolymers offer a sustainable material paradigm that incorporates low bulk density, adequate mechanical strength, and effective electromagnetic attenuation capabilities. These findings strongly support the potential use of this material as a high-performance functional structural element in advanced technology construction applications requiring 5G/6G infrastructure and EMI protection.

ARTICLE IN PRESS

Limitations and Future Research

When the obtained data are evaluated cumulatively, they confirm that the determined optimal parametric range (25% vermiculite and 11–13 M NaOH) offers a versatile solution for structural elements requiring a balance between lightness and mechanical strength, as well as advanced electromagnetic damping capability. In this context, the developed lightweight geopolymer composites have been found to have the potential for use as a high-performance and sustainable alternative in critical applications such as interior panel systems, electromagnetic barrier layers, and non-load-bearing

ARTICLE IN PRESS

structural components. Consequently, this study provides an empirical roadmap for the design of functional construction materials that both preserve structural integrity and minimize millimeter-wave interference.

Although this study empirically demonstrated the millimeter-wave screening potential of lightweight geopolymer composites, the operational continuity of the results achieved has not yet been fully characterized. Future research should focus on the long-term durability performance of the material under extreme environmental conditions such as freeze-thaw cycles, thermal aging, and chemical corrosion. Considering vermiculite's highly porous morphology, it is essential to investigate the effect of moisture diffusion and water absorption on mechanical integrity and dielectric stability. Furthermore, to verify performance consistency when scaling up from laboratory-scale mortar samples to industrial dimensions, large-scale structural elements must be tested in real EMC environments and across a broader frequency spectrum. Finally, to optimize the intrinsic balance between mechanical strength and SE, it is recommended to develop advanced material design approaches such as hybrid filler systems, fiber reinforcements, or vermiculite surface modification strategies.

ARTICLE IN PRESS

Data Availability

The datasets used and/or analyzed during the current study are available from the corresponding author on reasonable request.

Funding Declarations

This research received no external funding. No APC funding was provided by the authors' affiliated institution.

Conflict of Interest

The authors declare that they have no known competing financial interests or personal relationships that could have appeared to influence the work reported in this paper.

Acknowledgments

ARTICLE IN PRESS

This study was funded by the Scientific Research Projects Unit of Kayseri University under grant number FCD-2025-1234. The materials and experimental environments used in the publication were supported by the project.

References

[1] Çifci A. Electromagnetic Interference Shielding Properties of Vermiculite Doped Rigid Polyurethane Materials. Science of Advanced Materials. 2020;12:1833-8.
[2] Valberg, P. A. (2015). Electromagnetic Waves (EMF and RF) and Health Effects. Hamilton & Hardy's Industrial Toxicology, 1069-1086.
[3] Moon, J. H. (2020). Health effects of electromagnetic fields on children. Clinical and experimental pediatrics, 63(11), 422.
[4] Bandara, P., & Carpenter, D. O. (2018). Planetary electromagnetic pollution: it is time to assess its impact. The Lancet Planetary Health, 2(12), e512-e514.
[5] Esmailzadeh, S., Delavar, M. A., Aleyassin, A., Gholamian, S. A., & Ahmadi, A. (2019). Exposure to electromagnetic fields of high voltage overhead power lines and female infertility. The international journal of occupational and environmental medicine, 10(1), 11.
[6] Lewis, R. C., Hauser, R., Maynard, A. D., Neitzel, R. L., Wang, L., Kavet, R., & Meeker, J. D. (2016). Exposure to power-frequency magnetic fields and the risk of infertility and adverse pregnancy outcomes: update on the human evidence and recommendations for future study designs. Journal of toxicology and environmental health, Part B, 19(1), 29-45.
[7] Cherry, N. J. (2001). Evidence that electromagnetic fields from high voltage powerlines and in buildings, are hazardous to human health, especially to young children.
[8] Valjus, J. (1996). Health risks of electric and magnetic fields caused by high-voltage systems in Finland. Scandinavian journal of work, environment & health, 85-93.
[9] Pavlík, M., Bereš, M., & Beňa, Ľ. (2024). The influence of various commonly used building materials on the shielding effectiveness, reflection and absorption of the electromagnetic wave. Applied Sciences, 14(6), 2521.
[10] Vizi, G. N., & Vandenbosch, G. A. (2016). Building materials and electromagnetic radiation: The role of material and shape. Journal of Building Engineering, 5, 96-103.
[11] Mannan, M., Weldu, Y. W., & Al-Ghamdi, S. G. (2020). Health impact of energy use in buildings: Radiation propagation assessment in indoor environment. Energy Reports, 6, 915-920.
[12] Wahba, A. S., Elboushi, A., El-Sherbiny, Y. M., & El-Shazly, M. (2021). Electromagnetic energy in buildings: analysis of the effect of roof shape and treated materials. Journal of Building Performance Simulation, 14(5), 536-553.
[13] Davidovits, J. (2013). Geopolymer cement. A review. Geopolymer Institute, Technical papers, 21, 1-11.
[14] Mohmmad, S. H., Shakor, P., Muhammad, J. H., Hasan, M. F., & Karakouzian, M. (2023). Sustainable alternatives to cement: synthesizing metakaolin-based geopolymer concrete using nano-silica. Construction Materials, 3(3), 276-286.
[15] Soares, G. A., Bezerra, B. P., Antoniazzi, J. G., Innocentini, M. D. M., Marangon, E., & Luz, A. P. (2025). Physico-mechanical and thermal behavior of foamed mortars bonded with Portland cement or metakaolin-based geopolymer. Journal of Building Engineering, 111, 113644.

ARTICLE IN PRESS

ARTICLE IN PRESS

[16] Ünsal, Z., Ekinci, M. Ö., İlcan, H., Şahin, O., Selçuk, S., & Şahmaran, M. (2025). Life cycle assessment of geopolymer materials utilizing construction and demolition waste. Environmental Research, 122359.
[17] Uzer AU, Tunç U, Acar MC, Çelik AİJSE, Mechanics. Sustainable stabilization of clay soils using fly ash and blast furnace slag-based geopolymers: Comprehensive experimental evaluation and artificial neural network modelling. 2025;96:13.
[18] Tunç U, Kaya Z, Çelik Aİ. Sustainable high-performance injection geopolymers, role of GGBFS and water-to-binder ratio in strength, microstructure, and predictive modeling. Scientific Reports. 2025;15:42702.
[19] Costa, L. M., de Souza, T. D. C. C., de Oliveira, R. K. F. G., Almeida, N. G. S., & Houmard, M. (2025). Effects of silicas and aluminosilicate synthesized by sol-gel process on the structural properties of metakaolin-based geopolymers. Applied Clay Science, 267, 107743.
[20] Li, J., Song, K., Tao, Y., Cao, W., Wang, Y., & Yi, C. (2025). Production and optimization of sustainable, economical and sulphate-resistant binary geopolymers with a large sugarcane bagasse ash addition. Construction and Building Materials, 467, 140368.
[21] Hao, Q., Liu, S., Liu, Z., Takasu, K., Paine, K., Ke, X., & Suyama, H. (2025). Factors influencing the performance of biomass fly ash-based geopolymers. Construction and Building Materials, 489, 142415.
[22] Zwanenburg C, Konstadinou M, Meijers P, Goudarzy M, König D, Dyvik R, et al. Assessment of the dynamic properties of holocene peat. Journal of Geotechnical and Geoenvironmental Engineering. 2020;146:04020049.
[23] Çelik Aİ, Karalar M, Tunç U, Şahan MF, Althaqafi E, Umiye OA, et al. Mechanical and impact behavior of lightweight geopolymer concrete produced by pumice and waste rubber. 2025;15:35280.
[24] Wang, T., Ning, X., Yang, L., Rao, F., & Jiang, K. (2025). The synthesis of an iron tailings-based geopolymer with synergistic electromagnetic wave consumption property. Environmental Research, 268, 120744.
[25] Kim, C., & Lee, B. (2025). Multifunctional role and potential of vermiculite as a natural two-dimensional nanomaterial in a variety of advanced applications. Environmental Engineering Research, 30(5).
[26] Li, S., Li, X., Liang, Y., Shi, J., Du, Y., Chen, W., ... & Xia, C. (2025). Full-Lifecycle Biocarbon Foam through Multiscale Pore Engineering Toward Ultra-High Electromagnetic Absorption. Advanced Functional Materials, e13375.
[27] Lu, W., Wang, J., Wang, M., Yan, J., Mao, D., & Hu, E. (2025). Nanoparticle-Enhanced Phase Change Materials (NPCMs) in Solar Thermal Energy Systems: A Review on Synthesis, Performance, and Future Prospects. Energies, 18(17), 4516.
[28] Shen, T., Zhu, B., Shen, Y., Zhang, X., Shi, C., Zhang, K., & Tian, W. T. In-Situ Growth of Cual-Ldhs on Vermiculite Nanolayers for Assembling Thermostable and Anti-Bacterial Films. Available at SSRN 5246094.
[29] Ray, S. S., Tersur Orasugh, J., & Temane, L. T. (2025). Structure and Properties of Natural Nanoclays. In Nanoclays: Materials Properties and Advanced Applications (pp. 33-72). Cham: Springer Nature Switzerland.
[30] Upadhyay, R. K. (2025). Non-metallic minerals and their deposits. In Geology and Mineral Resources (pp. 563-652). Singapore: Springer Nature Singapore.
[31] Kayabaşı R, Çelik Aİ, Uzer AU, Tunç U, Şener A. Effect of expanded vermiculite and binder ratios on fire resistance and mechanical properties of sustainable lightweight geopolymer concretes. Powder Technology. 2026;469:121729.
[32] Selvaraj, V. K., Subramanian, J., Mouleswaran, S., Keerthan, T. K., Muneeswaran, T., Nath, A. K., & Raju, M. P. (2025). Sustainable development of bioepoxy composites reinforced with recycled rigid polyurethane foam for mechanical, thermal, acoustic, and electromagnetic applications in a circular economy approach. Scientific Reports, 15(1), 8295.

ARTICLE IN PRESS

[33] Kholmurodova, S., Turaev, K. K., Alikulov, R., Beknazarov, K., Nomozov, A., & Eshmurodov, E. K. (2025). Obtaining an organic-inorganic sorbent based on vermiculite modified with urotropin and hydrolyzed polyacrylonitrile. Chemical Review and Letters, 8(2), 267-279.
[34] Hou, L., Xing, B., Zeng, H., Kang, W., Guo, H., Cheng, S., ... & Zhang, C. (2022). Aluminothermic reduction synthesis of Si/C composite nanosheets from waste vermiculite as high-performance anode materials for lithium-ion batteries. Journal of Alloys and Compounds, 922, 166134.
[35] Tekin, İ., & Pekgöz, M. (2025). Effect of different fiber reinforcements on the electromagnetic performance and mechanical properties of zeolitic tuff/calcite-based geopolymer composites. Journal of Building Engineering, 112874.
[36] Maestre, C. V., & Santos, G. N. (2023). Effect of bismuth oxide nanoparticle on the electromagnetic interference shielding and thermal stability of industrial waste based-geopolymer composites. Scientific Reports, 13(1), 1787.
[37] Al-Buriahi, M. S., Alzahrani, J. S., Owoeye, S. S., Yılmaz, E., & Çalıskan, F. (2025). Fabrication, physical properties and radiation shielding performance of geopolymers reinforced by B2O3: Eco-friendly building material. Radiation Physics and Chemistry, 112982.
[38] Nguyen, V. V., Le, V. S., Louda, P., Szczypiński, M. M., Ercoli, R., Růžek, V., ... & Buczkowska, K. E. (2022). Low-density geopolymer composites for the construction industry. Polymers, 14(2), 304.
[39] Wu, Y., Wang, Y., Liu, X., & Ma, G. (2023). Effects of layered and metasurface structures on the electromagnetic wave absorption performance of cementitious materials. Journal of Building Engineering, 72, 106719.
[40] Ozturk M, Sevim UK, Akgol O, Unal E, Karaaslan M. Investigation of the mechanic, electromagnetic characteristics and shielding effectiveness of concrete with boron ores and boron containing wastes. Construction and Building Materials. 2020;252:119058.
[41] KK, Y., Begum, S., Kumar, G. P., Reddy, K. H. K., Bhargavi, K. S., S, G., & M, D. H. (2025). Development of lightweight high-strength engineered geopolymer composites using slag waste and vermiculite powder: mechanical, durability and microstructural assessments. Emergent Materials, 1-28.
[42] Bhayat, M. T., Babafemi, A. J., & De Villiers, W. (2025). Performance and Sustainability of Ambient-Cured One-Part Fly Ash and Slag-Based Geopolymer Concrete Masonry Units Incorporating Expanded Vermiculite. Advances in Civil Engineering, 2025(1), 7440021.
[43] ÇELİK, A. İ., KAYABAŞI, R., UZER, A. U., TUNÇ, U., & ŞENER, A. Fire Resistance and Mechanical Properties of Light Weight Geopolymer Concrete Based on Expanded Vermiculite: Performance Prediction by Taguchi and Anova. Available at SSRN 5164563.
[44] Maiti, S., Jain, N., Malik, J., & Baliyan, A. (2023). Light weight plasters containing vermiculite and FGD gypsum for sustainable and energy efficient building construction materials. Journal of The Institution of Engineers (India): Series A, 104(3), 603-614.
[45] Asim, N., Alghoul, M., Mohammad, M., Amin, M. H., Akhtaruzzaman, M., Amin, N., & Sopian, K. (2019). Emerging sustainable solutions for depollution: Geopolymers. Construction and building materials, 199, 540-548.
[46] Emdadi, Z., Asim, N., Ambar Yarmo, M., Shamsudin, R., Mohammad, M., & Sopian, K. (2016). Green material prospects for passive evaporative cooling systems: Geopolymers. Energies, 9(8), 586.
[47] Singh, N., Raza, J., Colangelo, F., & Farina, I. (2024). Advancements in lightweight artificial aggregates: typologies, compositions, applications, and prospects for the future. Sustainability, 16(21), 9329.

ARTICLE IN PRESS

[48] Suraneni P, Burris L, Shearer CR, Hooton RD. ASTM C618 fly ash specification: Comparison with other specifications, shortcomings, and solutions. ACI Mater J. 2021;118:157-67.
[49] Pourkhorshidi AR, Najimi M, Parhizkar T, Jafarpour F, Hillemeier B. Applicability of the standard specifications of ASTM C618 for evaluation of natural pozzolans. Cement and Concrete Composites. 2010;32:794-800.
[50] Organik. Vermiculite. 2025.
[51] Sahin, S., Nahar, N. K., & Sertel, K. (2020). A simplified Nicolson–Ross–Weir method for material characterization using single-port measurements. IEEE Transactions on Terahertz Science and Technology, 10(4), 404-410.
[52] Angiulli, G., & Versaci, M. (2021). Retrieving the effective parameters of an electromagnetic metamaterial using the Nicolson-Ross-Weir method: An analytic continuation problem along the path determined by scattering parameters. IEEE Access, 9, 77511-77525.
[53] Park HH. Electromagnetic shielding analysis of planar materials using ASTM D4935 standard fixture. IEEE Transactions on Electromagnetic Compatibility. 2022;64:1767-78.
[54] Norma A. C109/C109M, Standard Test Method for Compressive Strength of Hydraulic Cement Mortars (Using 2-in. or [50-mm] Cube Specimens), West Conshohocken, Pa. EE UU): American Society for Testing and Materials. 1999.
[55] ASTM International WC, PA. . ASTM C348-20. Standard Test Method for Flexural Strength of Hydraulic-Cement Mortars. . 2020.
[56] Davidovits J. Geopolymer chemistry and applications: Geopolymer Institute, 2008.
[57] Rajan MS, AnuPriya A. Development and properties of low-calcium fly ash-based geo polymer concrete. Int J Innov Res Adv Eng. 2024;11:465-9.
[58] Gencel O, Koksal F, Sahin M, Durgun MY, Lobland HEH, Brostow W. Modeling of thermal conductivity of concrete with vermiculite by using artificial neural networks approaches. Experimental Heat Transfer. 2013;26:360-83.
[59] Öz A, Bayrak B, Kavaz E, Kaplan G, Çelebi O, Alcan HG, et al. The radiation shielding and microstructure properties of quartzic and metakaolin based geopolymer concrete. Construction and Building Materials. 2022;342:127923.
[60] Doğan-Sağlamtimur N, Bilgil A, Ertürk S, Bozkurt V, Süzgeç E, Akan AG, et al. Eco-geopolymers: Physico-mechanical features, radiation absorption properties, and mathematical model. Polymers. 2022;14:262.
[61] Yılmaz N, Çelik A. Çapraz Kamalı Haddeleme Kalıp Tasarımında Uygulanması Gereken Kuvvet Üzerine Etki Eden Parametrelerin İncelenmesi. Gazi Üniversitesi Mühendislik Mimarlık Fakültesi Dergisi. 2013;28.
[62] Ranjit R. A primer on the Taguchi method: Society of Manufacturing Engineers. Estados Unidos: Society of Manufacturing Engineers. 2010:172-4.
[63] Korniejenko K, Pławecka K, Bulut A, Şahin B, Azizağaoğlu G, Figiela B. Development of lightweight geopolymer composites containing perlite and vermiculite. Journal of achievements in materials and manufacturing Engineering. 2023;117.
[64] Gencel O, Gholampour A, Tokay H, Ozbakkaloglu T. Replacement of natural sand with expanded vermiculite in fly ash-based geopolymer mortars. Applied Sciences. 2021;11:1917.
[65] Koksal F, Gencel O, Kaya M. Combined effect of silica fume and expanded vermiculite on properties of lightweight mortars at ambient and elevated temperatures. Construction and Building Materials. 2015;88:175-87.
[66] Kaya M, Köksal F. Physical and mechanical properties of C class fly ash based lightweight geopolymer mortar produced with expanded vermiculite aggregate. Revista de la construcción. 2022;21:21-35.